Resource

Molecular Cell

Dynamic Rewiring of Promoter-Anchored Chromatin Loops during Adipocyte Differentiation

Graphical Abstract

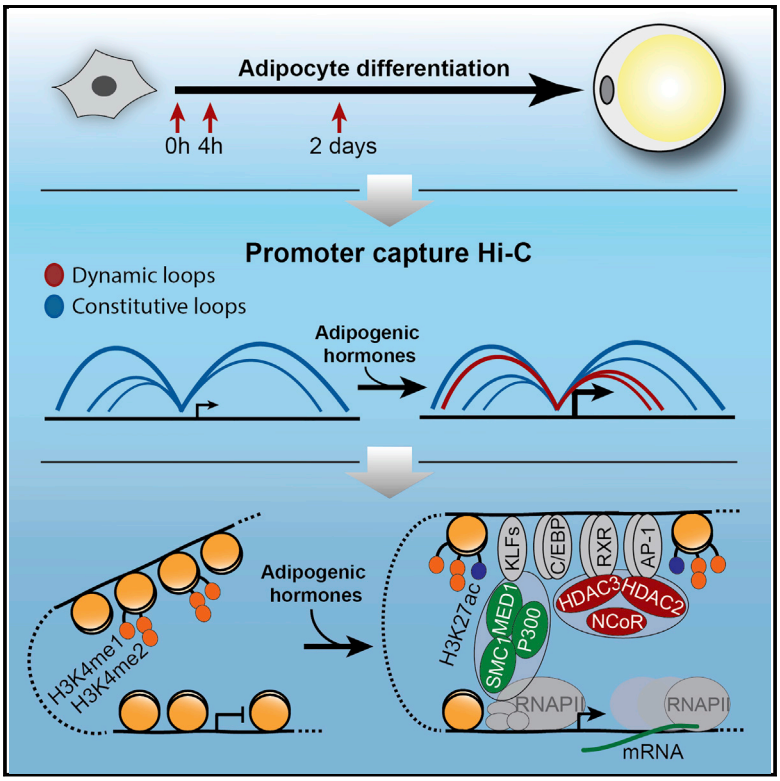

Authors

Rasmus Siersbæk,
Jesper Grud Skat Madsen,
Biola Maria Javierre, ...,
Mikhail Spivakov, Peter Fraser,
Susanne Mandrup

Correspondence

peter.fraser@babraham.ac.uk (P.F.),
s.mandrup@bmb.sdu.dk (S.M.)

In Brief

Siersbæk et al. demonstrate a rapid and dynamic rewiring of promoter-anchored chromatin loops during adipocyte differentiation, which is linked to changes in the activity of promoters and enhancers. Loop formation involves activation of poised enhancers and is associated with extensive recruitment of both coactivators and corepressors.

Highlights

- Dynamic promoters and enhancers are connected through dynamic chromatin loops
- Chromatin loop formation is coupled to activation of poised enhancers
- Enhancer activation is associated with corepressor recruitment

Siersbæk et al., 2017, Molecular Cell 66, 420–435
May 4, 2017
http://dx.doi.org/10.1016/j.molcel.2017.04.010

CellPress

CellPress

Molecular Cell
Resource

Dynamic Rewiring of Promoter-Anchored Chromatin Loops during Adipocyte Differentiation

Rasmus Siersbæk,[1,5,6] Jesper Grud Skat Madsen,[1,6] Biola Maria Javierre,[2,6] Ronni Nielsen,[1,6] Emilie Kristine Bagge,[1] Jonathan Cairns,[2] Steven William Wingett,[2,3] Sofie Traynor,[1] Mikhail Spivakov,[2] Peter Fraser,[2,4,*] and Susanne Mandrup[1,7,*]

[1]University of Southern Denmark, Campusvej 55, 5230 Odense M, Denmark
[2]Nuclear Dynamics Programme, Babraham Institute, Cambridge CB22 3AT, UK
[3]Bioinformatics Group, Babraham Institute, Cambridge CB22 3AT, UK
[4]Department of Biological Science, Florida State University, Tallahassee, FL 32306, USA
[5]Present address: Cancer Research UK Cambridge Institute, University of Cambridge, Li Ka Shing Centre, Robinson Way, Cambridge CB2 0RE, UK
[6]These authors contributed equally
[7]Lead Contact
*Correspondence: peter.fraser@babraham.ac.uk (P.F.), s.mandrup@bmb.sdu.dk (S.M.)
http://dx.doi.org/10.1016/j.molcel.2017.04.010

SUMMARY

Interactions between transcriptional promoters and their distal regulatory elements play an important role in transcriptional regulation; however, the extent to which these interactions are subject to rapid modulations in response to signals is unknown. Here, we use promoter capture Hi-C to demonstrate a rapid reorganization of promoter-anchored chromatin loops within 4 hr after inducing differentiation of 3T3-L1 preadipocytes. The establishment of new promoter-enhancer loops is tightly coupled to activation of poised (histone H3 lysine 4 mono- and dimethylated) enhancers, as evidenced by the acquisition of histone H3 lysine 27 acetylation and the binding of MED1, SMC1, and P300 proteins to these regions, as well as to activation of target genes. Intriguingly, formation of loops connecting activated enhancers and promoters is also associated with extensive recruitment of corepressors such as NCoR and HDACs, indicating that this class of coregulators may play a previously unrecognized role during enhancer activation.

INTRODUCTION

Gene regulatory elements such as enhancers are very abundant in the genome (Thurman et al., 2012) and are often located large distances away from their target gene promoters. Gene regulatory regions are known to be highly enriched for disease-associated genetic variants (Consortium et al., 2012; Maurano et al., 2012), which underscores the importance of understanding enhancer-driven gene regulation and accurately linking enhancers to their target genes.

Technological developments that allow identification of chromatin contacts at a genome-wide level (e.g., Hi-C (Lieberman-Aiden et al., 2009) and chromatin interaction analysis by paired-end tag sequencing (ChIA-PET; Fullwood et al., 2009) have provided unique insight into the 3D structure of chromatin in specific cells. The unbiased but relatively low-resolution approach of Hi-C has revealed that the genome is organized into topologically associating domains (TADs) of several hundred kilobases to a few megabases in size (Dixon et al., 2012; Nora et al., 2012). Furthermore, additional domains within TADs have been described, e.g., insulated neighborhoods (Dowen et al., 2014; Ji et al., 2016) and sub-TADs (Phillips-Cremins et al., 2013). The integrity of these domains has been shown to be important for genome organization and proper control of gene expression (Dowen et al., 2014; Ji et al., 2016; Lupiáñez et al., 2015; Nora et al., 2012; Zuin et al., 2014). TADs and insulated neighborhoods have been reported to be largely stable between cell types and in response to specific stimuli (Dixon et al., 2015, 2012; Dowen et al., 2014; Jin et al., 2013; Nora et al., 2012), although some studies suggest that TAD boundaries also have plastic properties (Krijger et al., 2016; Li et al., 2015). CTCF and cohesin are highly enriched at borders of TADs and insulated neighborhoods (Dixon et al., 2012; Dowen et al., 2014), where CTCF plays an important role in maintaining domain integrity (Dowen et al., 2014; Zuin et al., 2014).

ChIA-PET has provided important insight into the 3D organization of promoters and enhancers at much higher resolution (Fullwood et al., 2009; Heidari et al., 2014; Li et al., 2012) than what is currently feasible by Hi-C. Promoter-enhancer loops are largely organized by the Mediator and cohesin complexes, and these factors have been shown to demarcate active enhancers (Dowen et al., 2014; Kagey et al., 2010; Phillips-Cremins et al., 2013; Whyte et al., 2013; Yan et al., 2013), where they play important roles in bridging enhancers and promoters in 3D (Ing-Simmons et al., 2015; Malik and Roeder, 2010; Phillips-Cremins et al., 2013; Zuin et al., 2014). Little is known about the dynamics of such promoter-enhancer loops at high resolution. This is largely due to technical limitations, e.g., the complexity of Hi-C libraries requires ultra-deep sequencing in order to obtain sufficient resolution to study promoter-enhancer loops (Jin et al., 2013). Furthermore, ChIA-PET is biased by the factor-dependent

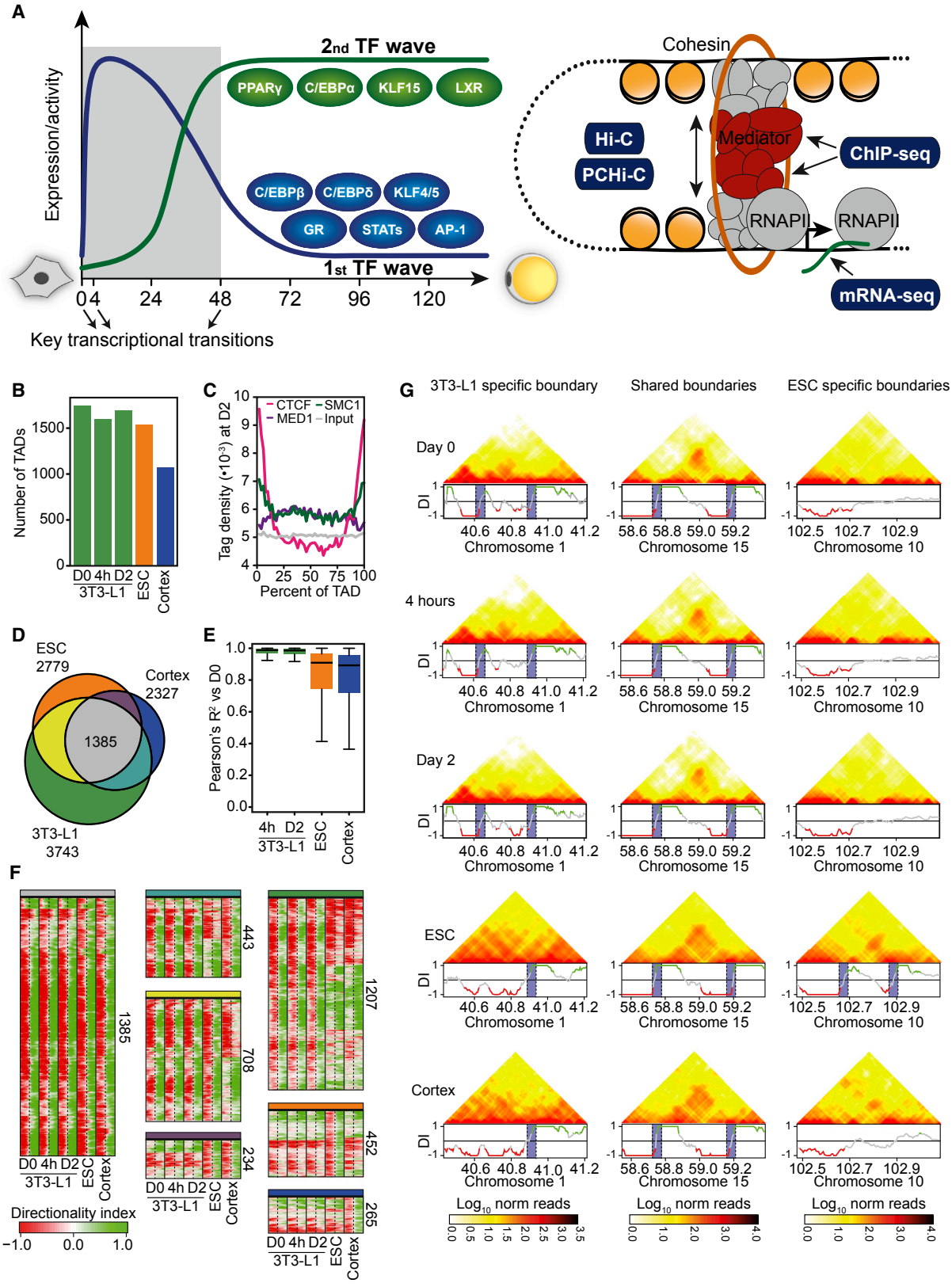

(legend on next page)

pull-down step and therefore cannot be used for studying changes in interactions.

Recently, promoter capture Hi-C (PCHi-C) was developed to allow identification of promoter-anchored chromatin loops at high resolution in different cells in an unbiased manner (Sahlén et al., 2015; Schoenfelder et al., 2015). Comparison of different cell types revealed clear differences in the organization of promoter-anchored chromatin loops between cell types, correlating with cell type-specific gene expression (Javierre et al., 2016). However, the degree to which chromatin looping is dynamically reorganized in response to pro-differentiation signals, for example, remains unclear. Only few studies have investigated the plasticity of promoter-enhancer loops in response to external stimuli so far. Based on ultra-deep sequencing of Hi-C libraries, it has been reported that in response to TNF-α stimulation, NF-κB is dynamically recruited to the genome, where it activates target gene programs, but this does not seem to be associated with a dramatic rewiring of the associated chromatin loops (Jin et al., 2013). Similarly, transcriptional changes during *Drosophila* development mainly occur in the context of pre-programmed chromatin loops (Ghavi-Helm et al., 2014). In contrast to these findings, studies testing a few selected binding sites of the estrogen receptor and the glucocorticoid receptor suggest that hormone stimulation increases chromatin loop formation between receptor-bound enhancers and target gene promoters (Fullwood et al., 2009; Pan et al., 2008; Stavreva et al., 2015).

Here we have employed Hi-C and PCHi-C in combination with comprehensive ChIP-seq and mRNA-seq analyses to investigate the dynamics of promoter-anchored chromatin loops during 3T3-L1 adipocyte differentiation. We demonstrate a rapid rewiring of these promoter-anchored loops and show that this is coupled to changes in the activity of the connected promoters and enhancers. Furthermore, analyses of factor recruitment at activated enhancers connected to activated genes indicate that corepressors may play a previously unrecognized role during enhancer activation.

RESULTS

TADs Are Stable during Adipocyte Differentiation

To obtain detailed insight into the dynamics of chromatin organization during cell differentiation, we used the 3T3-L1 preadipocyte cell line, which represents an attractive differentiation model as these cells undergo a very well-characterized differentiation process into mature lipid-laden adipocytes at a high rate (>95%) and in a synchronous manner upon stimulation with an adipogenic hormone cocktail. The transcriptional program driving 3T3-L1 differentiation can be divided into two waves of pro-adipogenic transcription factors (Figure 1A, left) (Siersbæk and Mandrup, 2011; Siersbæk et al., 2012). Activation of both waves is associated with dramatic reprogramming of local chromatin features, e.g., chromatin accessibility (Siersbæk et al., 2011) and epigenomic modifications (Mikkelsen et al., 2010; Steger et al., 2010). We focused our analyses on three key time points (Figure 1A, left): day 0, which represents the preadipocyte state, where the expression/activity of most of these pro-adipogenic factors is relatively low; 4 hr after induction of differentiation, where the expression/activity of the first wave factors is high and that of the second wave factors is still low; and day 2, which represents the start of the second wave that drives the terminal differentiation program.

Initially, we performed regular Hi-C using in-nucleus ligation (Figure 1A, right), which revealed >1,500 TADs with an average size of approximately 420 kb at all three time points (see Table S1 for overview of sequencing details). This number of TADs is similar to that found in other cell types such as embryonic stem cells (ESCs) (Figure 1B) (Battulin et al., 2015; Dixon et al., 2015, 2012). Consistent with the proposed roles of the architectural proteins MED1 and CTCF, ChIP-seq analysis revealed that CTCF is enriched at TAD borders, whereas MED1 is enriched toward the TAD center (Figure 1C). In contrast, SMC1 binds both in the center of the TAD as well as at the TAD boundaries in line with the proposed dual role of cohesin at TAD borders and promoter-enhancer interactions (Phillips-Cremins et al., 2013). Notably, analyses of the direction of chromatin interactions around TAD borders found in 3T3-L1 cells, ESCs, and cortex (Dixon et al., 2012) revealed that the TAD borders identified in 3T3-L1 cells are distinct from those observed in other cell types but remain largely constant at 50 kb resolution during differentiation (Figures 1D–1G). This indicates that the higher-order chromatin organization is preprogrammed in 3T3-L1 cells but remains relatively invariant throughout differentiation.

PCHi-C Identifies Allele-Selective Promoter-Enhancer Loops Regulating Allele-Selective Gene Expression

Having established that the higher-order chromatin architecture at the level of TADs remains relatively constant during differentiation, we sought to specifically delineate the dynamics of promoter-anchored chromatin loops by PCHi-C. The capture array enriched fragments containing at least one of >25,000 annotated mouse promoters (Sahlén et al., 2015; Schoenfelder et al., 2015), thereby allowing for genome-wide identification of promoter-anchored chromatin loops at high resolution by moderate sequencing depth.

Figure 1. TADs Do Not Change during 3T3-L1 Adipocyte Differentiation

(A) Schematic overview of the experimental approach. Peroxisome proliferator-activated receptor γ, PPARγ; CCAAT/enhancer-binding protein, C/EBP; Krüppel-like factor, KLF; liver X receptor, LXR; glucocorticoid receptor, GR; signal transducer and activator of transcription, STAT; activator protein 1, AP-1.

(B) Number of TADs identified at different time points during 3T3-L1 adipocyte differentiation and in embryonic stem cells (ESC) and cortex (Dixon et al., 2012) (GEO: GSE35156).

(C) Average ChIP-seq tag density for MED1, SMC1, and CTCF around TADs identified at day 2 of differentiation. TADs are scaled to the same size.

(D) Overlap between TAD boundaries identified at 50 kb resolution in 3T3-L1, ESC, and cortex.

(E) Correlation of TAD boundaries found in (D) between 3T3-L1 preadipocytes and later time points of differentiation/other cell types.

(F) Directionality index around TAD boundaries identified in (D). Directionality index is a measure of the overall direction of the interactions at a given genomic position based on Hi-C data (see STAR Methods for more details). Color code indicated above each heatmap is the same as in (D).

(G) Heatmap showing the interaction frequencies around different types of TADs. DI, directionality index.

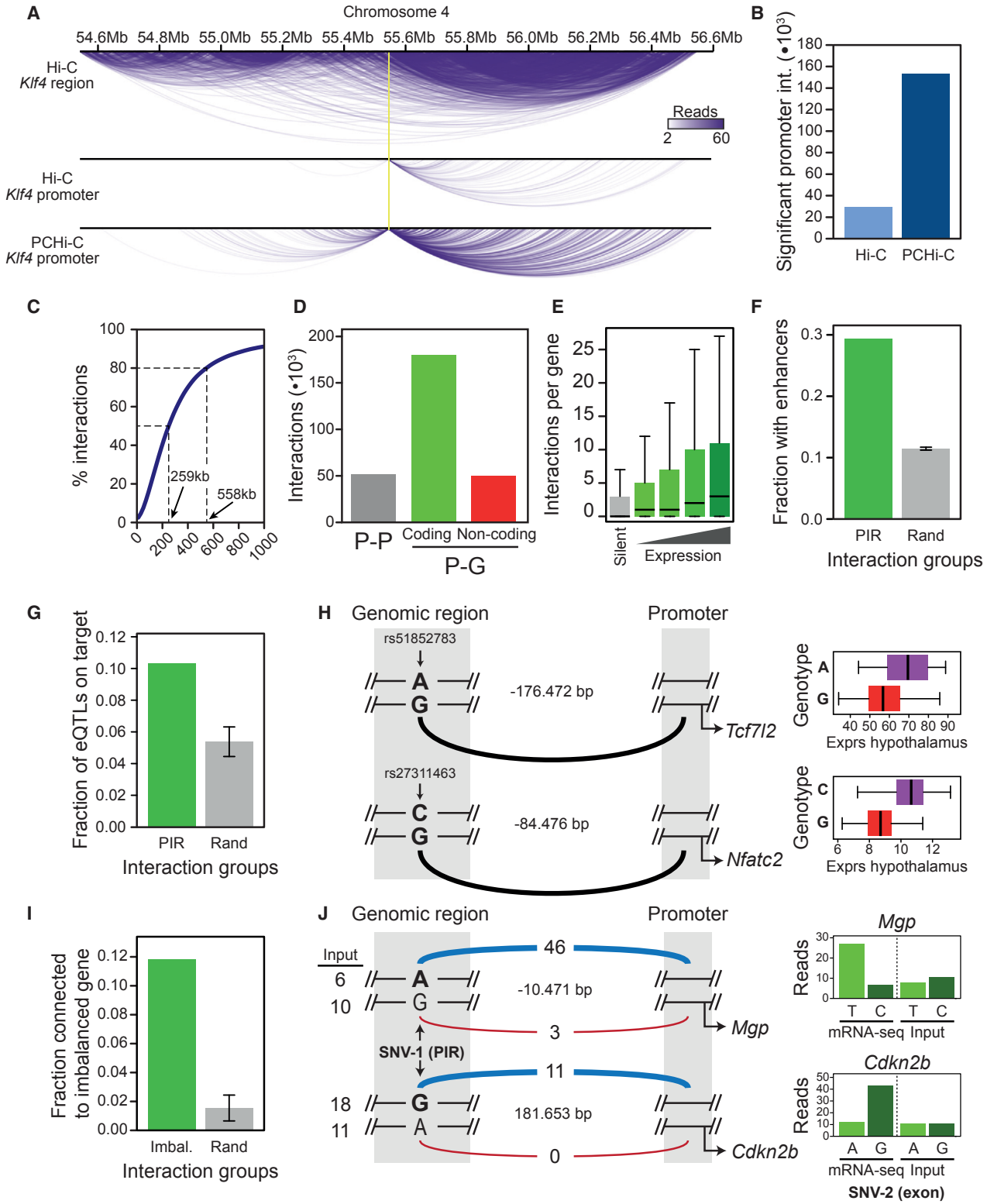

Figure 2. PCHi-C Identifies Functionally Important Promoter-Anchored Chromatin Loops

(A) Example of the increase in coverage of promoter-anchored chromatin loops in PCHi-C compared to regular Hi-C at the *Klf4* locus.

(B) Genome-wide differences in the number of significant promoter-anchored chromatin interactions called using Hi-C (called by HOMER; Heinz et al., 2010) and PCHi-C (called by CHiCAGO; Cairns et al., 2016). Libraries have been subsampled to the same size.

(legend continued on next page)

Two independent PCHi-C experiments with a total of 161–236 million unique valid sequence tags involving at least one promoter for day 0, 4 hr, and day 2 of 3T3-L1 differentiation revealed a clear increase in the coverage of promoter-anchored interactions compared to regular Hi-C (Figures 2A and 2B) and allowed us to identify more than 290,000 promoter-anchored chromatin loops at HindIII fragment resolution (average size of around 4 kb). As expected, these interactions are enriched within TADs, but many of them also span TAD boundaries (Figure S1A). Almost all the detected promoter-anchored interactions (98.5%) connect two HindIII fragments on the same chromosome (*cis* interactions) (Figure S1B), and 50% and 80% of these *cis* interactions span distances of less than 259 kb and 558 kb, respectively (Figure 2C). The majority (181,093) of interactions involve promoters of protein-coding genes (Figure 2D).

Notably, the number of promoter-interacting regions (PIRs) increases with the expression level of the gene (Figure 2E), indicating an overall activating function of the identified promoter-anchored chromatin loops for gene regulation. Consistently, analysis of PIRs shows that these regions are enriched for enhancer-associated features, as determined by ChIP-seq of MED1, SMC1, and P300, compared with distance-matched random regions (Figure 2F). This is in line with previous findings in ESCs and liver cells (Cairns et al., 2016; Schoenfelder et al., 2015) and indicates that many loops connect promoters and their respective enhancers. In further support of this, PIRs are enriched for previously identified eQTLs (Hasin-Brumshtein et al., 2016; Javierre et al., 2016) that are functionally linked to the same gene as the PIR compared to random distance-matched regions (Figure 2G and examples in Figure 2H). Importantly, by taking advantage of single nucleotide variants (SNVs) in PIRs and their connected promoters in 3T3-L1 cells, we demonstrate that allele-selective promoter-anchored chromatin loops are enriched for promoters driving allele-selective gene expression as determined by mRNA-seq (Figure 2I and examples in Figure 2J). Taken together, these analyses indicate that promoters loop to functionally important enhancers and demonstrate that differences in looping strength between alleles are associated with allele-selective gene expression in differentiating 3T3-L1 preadipocytes. This supports a functional gene regulatory role of the identified promoter-anchored interactions.

PCHi-C Reveals Dynamic Rewiring of Chromatin Loops

To determine the degree of plasticity of chromatin interactions identified by PCHi-C during differentiation, we subdivided all interactions based on the change in interaction strength as determined by tag counts (Figure 3A). Interestingly, 57.6% and 25.2% of the identified interactions change at least 1.5- or 2-fold, respectively, during the first 2 days of differentiation, with a similar proportion of interactions increasing and decreasing in strength. The same degree of plasticity was found when only analyzing promoter-interacting regions linking promoters to distal regions with enhancer features (i.e., MED1, SMC1, P300) as determined by ChIP-seq (Figure S1C).

To delineate the temporal dynamics of promoter-anchored chromatin loops in an unbiased manner, we took advantage of a recently described transformation of data series containing three data points (Stavreva et al., 2015), which is based on the color system hue-saturation-value (HSV) used in computer graphics (Figure 3B). After HSV transformation of the PCHi-C data (see STAR Methods), hue (i.e., the color tone spanning -180° to 180°) describes the temporal profile of the interaction strength, and the hue circle covers all possible temporal profiles in an unbiased manner (Figure 3B). Saturation is a measure of the maximum fold change (log2), and value is a measure of the maximum interaction strength (Figure 3B). Thus, HSV transformation makes strong and highly dynamic interactions appear as bright, colorful points in the hue circle, whereas weak and less dynamic interactions blend in with the background (see Figure 3 legend for more details).

The HSV transformation of PCHi-C data illustrates the rewiring of promoter-anchored chromatin loops described above (Figure 3A) and reveals that the two most prominent dynamic profiles of interaction strength are: (1) interactions that are weak or absent early in differentiation and strongest on day 2; and (2) interactions with a transient profile that peaks at 4 hr (Figure 3C). There are significantly more interactions with these temporal profiles that change $\geq$1.5-fold in strength during differentiation than is the case for all other interactions (Figure 3C, gray bars, $P_{adj} \leq 0.05$, Bonferroni corrected Z test). The promoters of fatty

(C) Cumulative percentage of promoter-anchored interactions spanning different genomic distances.

(D) All *cis* interactions identified by PCHi-C spanning $\leq$1 Mb are divided into groups based on the type of interaction. P-P denotes promoter-promoter interactions, whereas P-G denotes promoter-genome (non-promoter) interactions. Some baits contain multiple promoters (e.g., both non-coding and coding genes). In these cases, all interactions associated with that bait are assigned to both genes.

(E) Average number of interactions per promoter for genes with different expression levels as determined by mRNA-seq at day 0.

(F) Fraction of promoter-interacting regions (PIRs) and random HindIII fragments (Rand) that overlap enhancers as defined by ChIP-seq of MED1, SMC1, and P300. SD is indicated by error bars.

(G) Fraction of PIRs and random HindIII fragments that overlap previously identified eQTLs (Hasin-Brumshtein et al., 2016). SD is indicated by error bars.

(H) Two examples of previously identified eQTLs and the expression of their target genes in hypothalamus (right boxplot). The arc indicates the chromatin loop identified in 3T3-L1 cells between the eQTL and their target gene promoters.

(I) Fraction of imbalanced promoter-anchored chromatin loops (FDR-adjusted $P \leq 0.05$) (i.e., interactions with allele-selective loop formation; Imbal.) and random distance-matched HindIII fragments (Rand) that connect to promoters driving imbalanced genes (FDR-adjusted $P \leq 0.05$) (i.e., genes with allele-selective gene expression). SD is indicated by error bars.

(J) Examples of the association between allele-selective formation of promoter-anchored chromatin loops and allele-selective gene expression at the *Mgp* and *Cdkn2b* locus. Numbers to the left indicate normalized read counts in input DNA, whereas numbers on each loop indicate the normalized read counts in the PCHi-C data for the two alleles. Bar plot to the right shows the normalized read counts in the RNA-seq and input data for the two alleles. Allele-selective loop formation and gene expression are based on reads spanning the indicated SNPs in the PIR and an exon, respectively. Related to Figure S1.

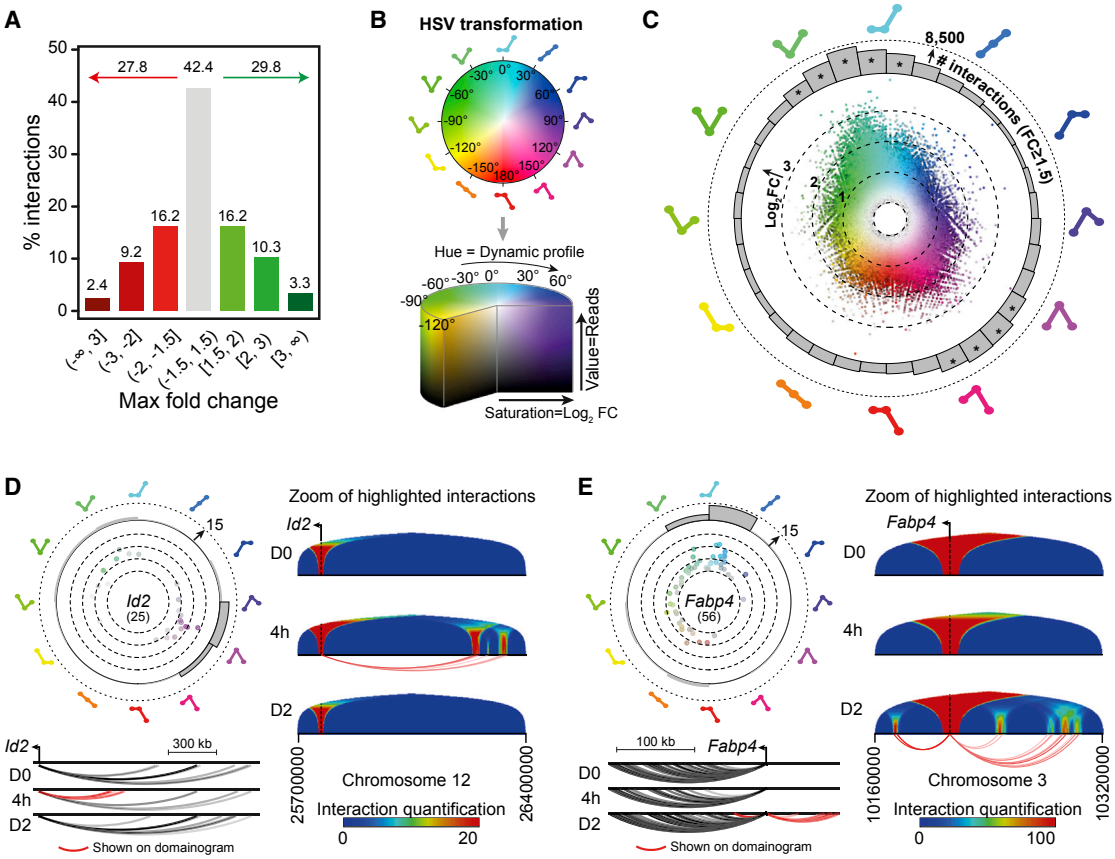

Figure 3. Dynamic Rewiring of Promoter-Anchored Chromatin Loops during 3T3-L1 Adipocyte Differentiation

(A) Fraction of interactions changing interaction strength as determined by tag counts during the course of differentiation.

(B) Schematic overview of hue-saturation-value (HSV) transformation. Hue spans −180° to 180° and describes the color tone in the HSV color system. In the HSV transformation of PCHi-C data, hue assigns a specific color to each interaction that exactly describes the temporal profile of the interaction. The hue circle thus contains all possible temporal interaction profiles in an unbiased manner. Saturation of the color is a measure of the maximum log2 fold change for the three time points, and value is a measure of the maximum interaction strength (based on tag counts) that determines the color brightness. In addition, the transparency of the color was also determined by the maximum interaction strength, i.e., weak interactions have a high transparency, whereas strong interactions have a low transparency. Strong and dynamic interactions are therefore represented as bright, colorful points, whereas weak or stable interactions are more white or black/transparent.

(C) HSV transformation of the 181,093 *cis* interactions connected to protein encoding genes. Interactions are visualized in a hue circle, where the distance from the center corresponds to the maximum log2 fold change. The histogram in the outer part of the circle shows the number of interactions in each bin that has a maximum fold change ≥ 1.5. *Dynamic interactions (fold change ≥ 1.5) in the hue bin are enriched over all other hue bins, $P_{adj} \leq 0.05$ (Bonferroni corrected Z test).

(D and E) Examples of gene promoters enriched for transient (*Id2*) (D) and late (*Fabp4*) (E) interactions, respectively. Top left, all interactions involving the indicated promoter are visualized in a hue circle. The number of interactions changed at least 1.5-fold in hue bins of 30° is indicated by bar plots. The number by the arrow and the dashed line in each plot indicates the span of the y axis, which describes the number of interactions in each bin. The total number of interactions for each gene is indicated below the gene name. Bottom left, overview of nearby interactions involving the indicated promoter. Right, virtual 4C analyses of nearby interactions involving the indicated promoter. These domainograms visualize the actual strength of the identified interactions based on the tag counts connecting the distal regions and the target promoter. Related to Figure S1.

acid binding protein 4 (*Fabp4*), which is a well-described adipocyte marker (Bernlohr et al., 1984; Graves et al., 1991), and inhibitor of DNA binding 2 (*Id2*), which has been shown to regulate early adipogenesis (Park et al., 2008), represent examples of gene promoters enriched for interactions with these two major temporal profiles (Figures 3D and 3E). Taken together, these results show a dynamic rewiring of promoter-anchored interactions during adipocyte differentiation and suggest that there are two major temporal profiles of reorganization of promoter-anchored chromatin loops that are concurrent with the activation of the first and second wave of adipogenic transcription factors, respectively. The formation of transient promoter-anchored chromatin loops at the 4 hr time point that are absent at day 2 is a particularly strong evidence of the plasticity of the 3D chromatin structure.

Rewiring of Chromatin Loops Is Coupled to Dynamic Changes in Gene Expression

To investigate whether the dynamics of promoter-anchored chromatin loops are coupled to changes in gene expression,

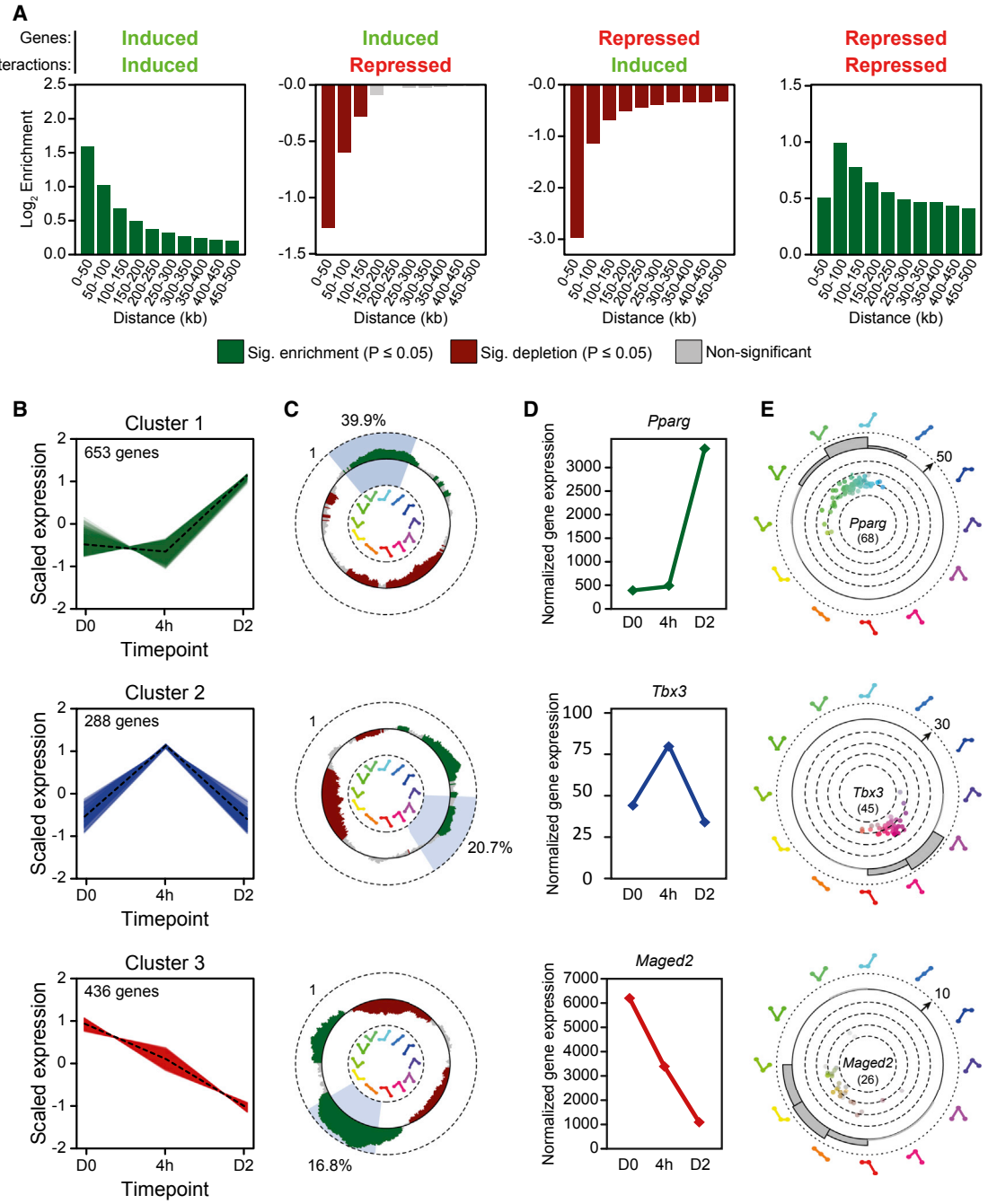

Figure 4. Gene Expression Dynamics Correlate with Changes in Strength of Nearby Interactions during 3T3-L1 Differentiation

(A) The enrichment/depletion of promoter-anchored interactions increasing and decreasing in strength (≥1.5-fold), respectively, at genes induced or repressed during the first 4 hr of differentiation is shown. Enrichment/depletion was calculated for interactions that span different genomic distances. Green and red colors indicate significant enrichment/depletion ($P \leq 0.05$, hypergeometric test).

(B) Fuzzy c-means clustering of mRNA-seq data from day 0, 4 hr, and day 2 of 3T3-L1 differentiation for genes with significant ($P_{adj} \leq 0.01$) changes in expression. Three of seven clusters are shown. The remaining clusters are shown in Figure S2B. Data are scaled and centered around 0. The dashed line indicates the mean of the cluster for each time point.

(C) Log2 enrichment/depletion of different interactions (spanning ≤ 100 kb) anchored at the promoters of genes in each cluster illustrated in a hue circle. Interactions associated with genes in each cluster were divided into hue bins, and the enrichment/depletion of interactions was calculated as described in STAR methods. Bins of 40° on the hue circle were moved 1° for each calculation of enrichment/depletion. The y axis spans −1 to 1 as indicated by the dashed lines. Green and red colors indicate significant enrichment/depletion (FDR-adjusted $P \leq 0.1$, binomial test). The blue shaded window on the hue circle corresponds to the range of dynamic changes in the gene expression cluster ± 10°, and the percentage of interactions falling in that window is indicated.

(legend continued on next page)

we initially focused on correlating interaction dynamics with promoter activity as determined by mRNA-seq during the first 4 hr of differentiation (Figure 1A, right). We found a strong correlation between changes in the strength of promoter-anchored chromatin loops and gene expression, i.e., induced genes are enriched for interactions that increase in strength and depleted for interactions that decrease in strength and vice versa for repressed genes (Figure 4A). Furthermore, changes in the strength of promoter-anchored interactions can predict changes in gene expression fairly well (Figure S2A), which is remarkable given the high number of interactions that connect to each gene promoter (Figure 2E).

To extend these findings to cover all the dynamic transitions during the first 2 days of differentiation (i.e., day 0, 4 hr, and day 2), we first identified the main temporal patterns of gene expression during this time frame using fuzzy c-means clustering of mRNA-seq data (Figures 4B and S2B). These gene clusters are enriched for the expected GO categories, e.g., the later cluster 1 and early cluster 2 are enriched for categories linked to fatty acid metabolism and fat cell differentiation, respectively (Figure S2C). For each gene cluster, we calculated the enrichment/depletion of dynamic interactions with different temporal profiles (hues) spanning $\leq$100 kb compared to constitutive genes and visualized this in a hue circle (Figures 4C and S2B). This analysis shows that promoters in all seven clusters are significantly enriched and depleted for interactions with specific temporal profiles, demonstrating that dynamic promoters are associated with dynamic chromatin loops in a non-random manner. Importantly, promoters in all clusters, especially promoters in clusters 1, 3, 4, and 7, are enriched for interactions with similar temporal profiles as the gene expression in each cluster, e.g., promoters of genes that are induced on day 2 (cluster 1) are significantly enriched for interactions that are strongest at that time point. This general association between the temporal changes in gene expression and promoter-anchored chromatin loops suggests a functional importance of these interactions. However, all promoter clusters also display enrichment of temporal interaction profiles that do not match the gene expression pattern of the cluster. For example, for the transient cluster 2, in addition to observing enrichment of transient interactions, we also find enrichment of interactions that are induced at 4 hr and maintained through day 2, showing that some chromatin loops persist after the transient burst in gene activation. Taken together, this shows that dynamic promoters are associated with a complex but non-random repertoire of interactions, with the one general observation that promoters in all clusters are significantly enriched for interactions with temporal profiles similar to the changes in gene expression. The promoter-anchored interactions for *Pparg*, T-Box 3 (*Tbox3*), and MAGE family member D2 (*Maged2*) provide representative examples of clusters 1 through 3, respectively (Figures 4D and 4E). The adipogenic cocktail leads to transient induction of a wide range of transcription factors (e.g., High-mobility group AT-hook 2 [HMGA2], vitamin D receptor [VDR], c-Jun), many of which have been shown to promote or modulate adipogenesis (Siersbæk et al., 2012). The compiled HSV plot of promoter-anchored interactions to genes encoding transiently induced transcription factors demonstrates enrichment for interactions with a similar profile (Figure S2D), indicating that the transient induction of these important genes is driven by dynamic chromatin looping. The above examples demonstrate how HSV plots of chromatin interactions with specific promoters (Figure 4E) represent a useful visualization method specifically highlighting the strongest and most dynamic interactions and their temporal profile. This can be used to predict which interactions/enhancers are likely to play the most dynamic role in transcriptional regulation of a given promoter in the context of many constitutive or modestly changing interactions.

In addition to the interactions between promoters and distal putative regulatory regions discussed above, we also identify 52,174 promoter-promoter interactions (Figure 2D), and these also show profound dynamic changes during differentiation similar to the interactions between promoters and non-promoter regions (Figure S2E). Interestingly, genes that are brought into close proximity by these promoter-promoter interactions are more often co-regulated than would be expected by chance (Figure S2F), indicating that these promoter-promoter interactions may also be functionally important. Taken together, these findings demonstrate that the dynamic changes in gene expression during the first 2 days of 3T3-L1 adipocyte differentiation are linked to dynamic changes in promoter-anchored chromatin loops with similar temporal profiles.

Rewiring of Promoter-Anchored Chromatin Loops Is Coupled to Enhancer and Super-enhancer Reprogramming

We showed above that PIRs are enriched for enhancers (Figure 2F). To investigate how changes in enhancer activity correlate with changes in interaction strength, we took advantage of our MED1 ChIP-seq data during differentiation (i.e., day 0, 4 hr, day 2, day 4, and day 7) (Figure 1A, right). We initially identified a merged set of super-enhancers (Whyte et al., 2013) based on MED1 ChIP-seq data from all time points. Interestingly, MED1 levels change significantly ($P \leq 0.05$) during differentiation at practically all these super-enhancers (99%), and clustering of the MED1 levels revealed five clusters with distinct temporal profiles (Figures 5A and 5B [clustering of day 0 through day 2] and Figures S3A and S3B [clustering of day 0 through day 7]). SMC1 binding shows similar dynamic changes as MED1 at all super-enhancer clusters (Figure S3C), demonstrating a dramatic and coordinated reprogramming of architectural proteins at super-enhancers during differentiation. Importantly, all clusters are enriched for binding of transcription factors that are active during the stage of differentiation where the activity of the super-enhancers peaks (Figure 5C; see Figure 1A for an overview of the temporal profile of transcription factor activity). This is consistent with the finding that the reprogramming of

(D) Expression of representative genes from each cluster in (B).

(E) All interactions associated with the promoters of the respective genes in (D) visualized in a hue circle. The number of interactions in 30° hue bins is illustrated by bar plots, and the span of the y axis is indicated by the number by the arrow and dashed line. The total number of interactions for each gene is indicated below the gene name. Related to Figure S2.

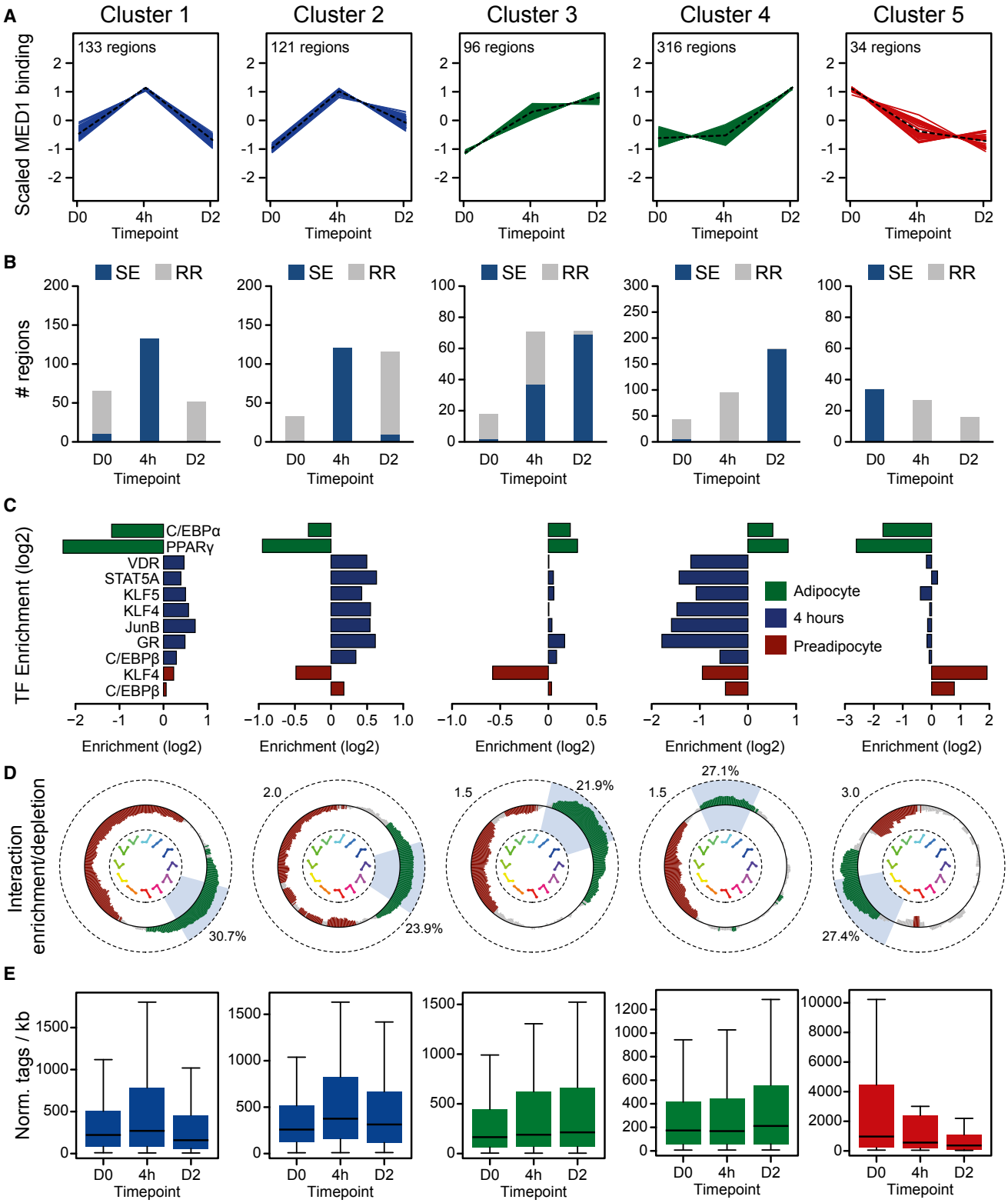

Figure 5. Extensive Reprogramming of Super-enhancers Correlates with Rewiring of Associated Chromatin Loops and Dynamic Regulation of Connected Genes

(A) Fuzzy c-means clustering of MED1 levels in significantly ($P_{adj} \leq 0.05$) changing merged super-enhancers was performed (see STAR Methods for more details). Log2 fold change of MED1 binding is shown. Data are scaled and centered on 0. Dashed line indicates the mean of the cluster at each time point.

(legend continued on next page)

super-enhancer during adipocyte differentiation is driven by the sequential and cooperative action of multiple adipogenic transcription factors (Siersbæk et al., 2011, 2014).

Importantly, we observe a strong correlation between the dynamics of MED1 binding at super-enhancers and the strength of interaction with target promoter(s) (Figure 5D). For example, super-enhancers that are established transiently at 4 hr are highly enriched for interactions with a transient peak in interaction strength at 4 hr, but greatly depleted for interactions with the opposite pattern. Importantly, the expression patterns of genes connected to super-enhancers within 100 kb from the promoter are strikingly similar to the dynamics of MED1 binding to the enhancer as well as the strength of the chromatin loops connecting the enhancer and the promoter (Figure 5E). Genes connected to dynamic super-enhancers include genes encoding key adipogenic transcription factors and metabolic enzymes, e.g., *Pparg*, *Cebpa*, *Cebpb*, *Fabp4*, Lipoprotein lipase (*Lpl*), Pyruvate carboxylase (*Pcx*), and Stearoyl-CoA desaturase 1 (*Scd1*). Similar coupling of dynamic changes in enhancer activity and interaction strength was found when analyzing all distal MED1 binding sites (Figures S3D–S3F). Taken together, these findings indicate that dynamic (super-)enhancers regulate their target genes, at least in part, through dynamic formation of chromatin loops.

H3K27ac and Coactivators, but Not H3K4me1 and -2, Are Good Predictors of Chromatin Loop Dynamics

A previous report has demonstrated that differences in H3K4me1 levels between cell types can predict cell-type-specific chromatin loops (Dixon et al., 2015). To address the role of different epigenomic marks in rewiring chromatin loops in response to adipogenic hormones, we initially used a combination of DNase-seq (Siersbæk et al., 2011) and H3K4me1 and -2 ChIP-seq in preadipocytes (time point 0) and 4 hr after induction of differentiation to define 9,505 putative enhancer regions that are connected to a target promoter through chromatin looping as determined by PCHi-C. These regions were further subdivided based on changes in activity as determined by H3K27ac (Figures S4A and S4B). As expected, regions with increased H3K27ac levels (i.e., activated enhancers) in response to adipogenic hormones are significantly enriched and depleted at interactions increasing and decreasing in strength, respectively (Figure S4C). The opposite pattern of enrichment/depletion is observed for regions with decreased H3K27ac levels. In contrast, regions with constant H3K27ac levels are not significantly associated with dynamic interactions. Interestingly, in contrast to H3K27ac, the levels of H3K4me1 and -2 do not change at activated or repressed enhancers engaging in promoter-anchored loops (Figures S4A and S4B). This indicates that the H3K4me1 mark, although it has been reported to follow cell-type-specific interactions (Dixon et al., 2015), is generally not correlated with the rapid modulations of chromatin interactions during 3T3-L1 differentiation.

These findings led us to investigate more directly how well different factors known to play a role in transcriptional regulation predict dynamic changes in chromatin loop formation. In addition to the epigenomic marks used above, we also included the architecture proteins MED1 and SMC1 as well as the acetyltransferase P300, deacetylases HDAC2 and -3, and the corepressor NCoR, which is linked to recruitment of HDAC3 (Watson et al., 2012). For each factor, we constructed a receiver operating characteristic (ROC) curve to investigate how well changes in binding of that factor, as determined by ChIP-seq, predict changes in chromatin loop formation (see STAR Methods for details). In line with the findings above, H3K27ac is the best, whereas H3K4me1 and -2 are the worst predictors of interaction dynamics (Figures 6A and 6B). Consistent with this, <10% of the dynamic interactions marked by H3K4me1 and -2 are associated with changes in the levels of H3K4me1 and -2 compared to approximately 60% for H3K27ac (Figure 6C and Figure S4D). Furthermore, whereas super-enhancers that are activated within the first 4 hr of differentiation are associated with increased levels of H3K27ac as well as coactivators and transcription factors, levels of H3K4me1 and -2 are constitutively high (Figures 6D and S4E). Thus, although H3K4me1 and -2 may play important roles in enhancer establishment, these marks do not seem to play a major role in the rapid dynamic regulation of promoter-enhancer interactions in response to pro-differentiation signals. This suggests that rewiring of promoter-enhancer loops in response to adipogenic hormones primarily occurs through activation of poised enhancers that are pre-programmed by H3K4me1 and -2 rather than through establishment of enhancers de novo.

Enhancer Activation, Loop Formation, and Gene Activation Are Associated with Extensive Corepressor Recruitment

The prediction analyses described above demonstrate that in addition to H3K27ac, a change in binding of any of the three coactivators (i.e., MED1, SMC1, and P300) or of any of the corepressors (i.e., HDAC2, -3, and NCoR) is also a fairly good predictor of interaction dynamics, indicating that these factors may play an important role in regulating promoter-enhancer loop formation. This led us to investigate the direction of regulation by these factors (Figure 6C). Surprisingly, the percentage of binding sites involved in dynamic interactions, where there is an equidirectional change in factor binding and chromatin loop

(B) The binary classification of the merged set of super-enhancers from (A) as super-enhancers (SE) or regular MED1 binding regions (RR) at each time point during the first 2 days of differentiation.

(C) Enrichment/depletion of transcription factor (TF) binding in each super-enhancer cluster compared to the other clusters. ChIP-seq data for different time points of differentiation were obtained from Siersbæk et al. (2011), (2014), and Step et al. (2014).

(D) Log2 enrichment/depletion of promoter-anchored interactions involving the identified super-enhancers, which span $\leq$100 kb, is shown in a hue circle. Enrichment/depletion for each bin was calculated as described in STAR Methods. Bins of 40° were moved 1° along the hue circle for each calculation. The number by the dashed line in each plot indicates the span of the y axis. Green and red colors indicate significant enrichment/depletion (FDR-adjusted $P \leq 0.1$, binomial test). The blue shaded window on the hue circle indicates the span of the dynamic changes in MED1 binding (±10°). The percentage of interactions in that window is indicated.

(E) The expression profile (shown as normalized [Norm.] tags per kb) of genes connected to super-enhancers in each cluster. Related to Figure S3.

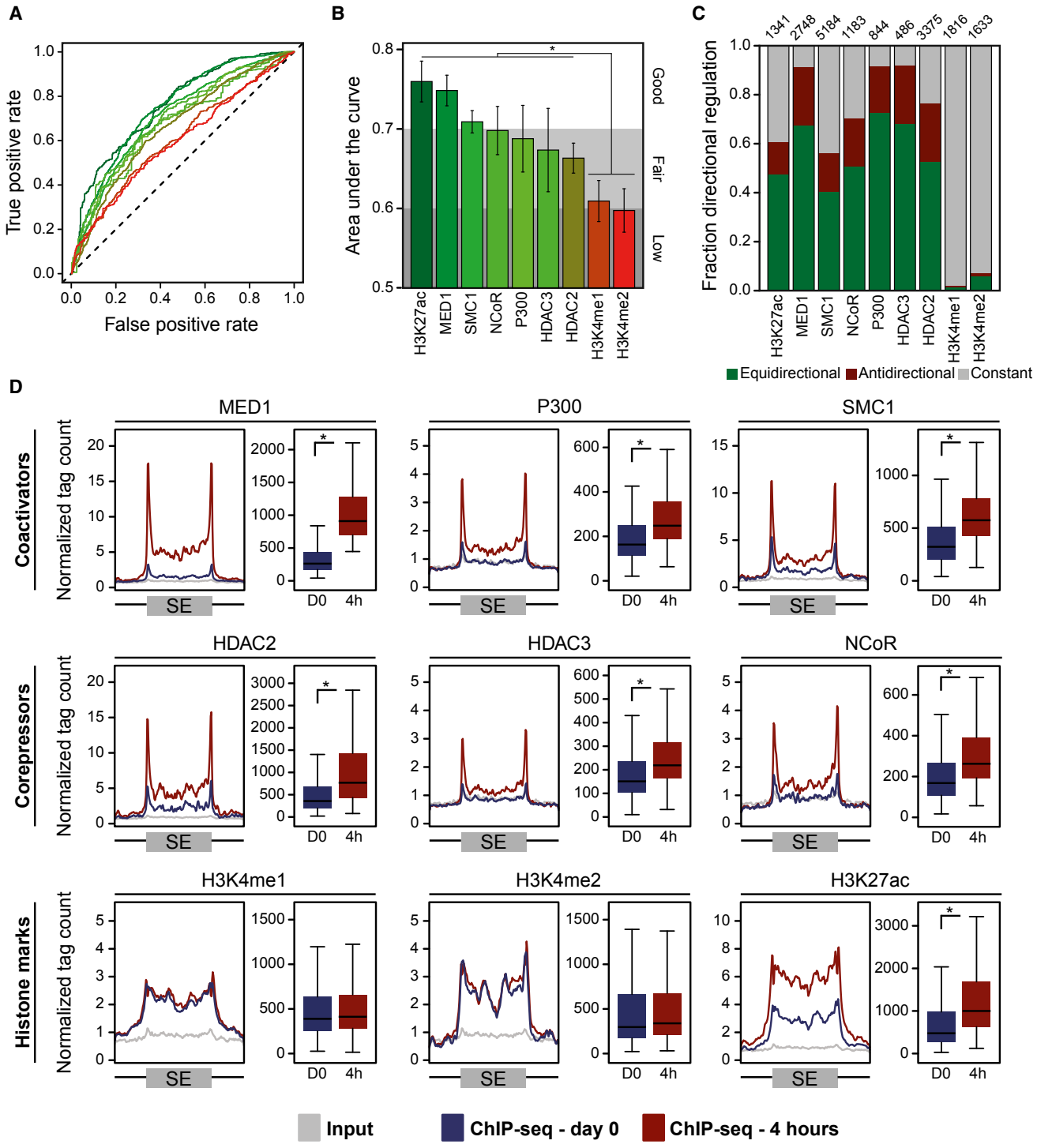

Figure 6. H3K27ac, Coactivators, and Corepressors, but Not H3K4me1/2, Can Predict Dynamic Promoter-Enhancer Interactions in 3T3-L1 Cells

(A) ROC curves for prediction of the dynamics of chromatin loops were constructed for each factor/mark by determining true and false positive rates at various thresholds for the fold change in ChIP signal. Only interactions associated with ChIP-seq signal for the investigated factor are included in the analyses. The 4 hr ChIP-seq samples for the histone marks (i.e., H3K4me1, H3K4me2, and H3K27ac) were published previously (Siersbæk et al., 2014), and the ChIP-seq on day 0 for these marks reported here were performed in parallel with these previously published samples.

(B) Area under the curve for the ROC curves in (A). Error bars denote the 95% confidence interval. *P $\leq$ 0.05, bootstrapping.

(legend continued on next page)

formation (i.e., binding and interaction strength change in the same direction), is high for both corepressors and coactivators (i.e., 40%–70%). Similarly, the percentage of sites with antidirectional change is low for both classes of coregulators (i.e., approximately 10%–20%). This indicates that recruitment of corepressors, similar to recruitment of coactivators, is associated with an increase in promoter-anchored chromatin looping.

To investigate the role of coregulators in rewiring promoter-anchored chromatin interactions in more detail, we first constructed a composite score for changes in binding of corepressors (i.e., HDAC2, -3, and NCoR) and coactivators (i.e., MED1, SMC1, and P300). This composite score provides a general measure of binding dynamics of these two distinct classes of coregulators (see STAR Methods for more details). Consistent with the findings above, when analyzing all regions bound by at least one coregulator on at least one time point, we find a strong direct correlation between the composite scores of corepressors and coactivators (Figures 7A and S5A), e.g., 20,437 out of 20,709 (98.7%) regions that gain binding of all three coactivators also gain binding of all three corepressors (Figure S6A). This direct correlation between the dynamics of corepressor and coactivator binding is also evident when analyzing individual corepressor/coactivator pairs (Figure S6B). Importantly, the dynamics of corepressor/coactivator binding is associated with a similar dynamic recruitment of transcription factors known to play important roles during early adipocyte differentiation, e.g., C/EBPs, KLF4, and RXR (Figure S5B). Pairwise comparison of changes in coregulator and transcription factor binding did not reveal any specific associations between factors (Figure S5C), indicating that the concerted action of these transcription factors may be important for recruiting both coactivators and corepressors to chromatin.

Consistent with the prediction analyses above, regions that gain both corepressor and coactivator binding during the first 4 hr of differentiation are associated with promoter-anchored loops that increase in strength, and vice versa for regions that have decreased binding of corepressors and coactivators (Figure 7B). Importantly, the target genes connected to these shared coactivator/corepressor binding regions through looping of the intervening chromatin tend to be regulated similarly to the chromatin loops, i.e., genes connected to enhancers that gain both corepressors and coactivators tend to be induced, whereas those that loop to enhancers that lose coactivator and corepressor binding are generally repressed (Figure 7C). An example of corepressor recruitment to an activated enhancer and concomitant formation of a promoter-enhancer loop and gene activation is shown for *Cebpb* in Figure 7D. Consistent with these findings, the binding of all investigated corepressors is highly induced at the activated enhancers linked to the formation of chromatin loops described in Figures S4A–S4C, similar to what is observed for coactivators and transcription factors known to play important roles during early differentiation (Figure S7). Furthermore, corepressor binding is highly induced in response to adipogenic hormones at early activated super-enhancers (Figure 6D), which activate target gene expression through the formation of promoter-enhancer loops (Figures 5D and 5E). Taken together, this suggests that corepressors may play an important yet unrecognized role in gene activation by regulating enhancer activation and chromatin loop formation. Furthermore, it indicates that in this system acute loss of gene activity mainly occurs through decommissioning of active enhancers rather than active repression involving recruitment of corepressors.

DISCUSSION

The degree to which promoter-enhancer loops are hardwired in the genome or change in response to signals in a given cell type constitutes a major question in transcriptional regulation. The few previous studies addressing this issue (Fullwood et al., 2009; Ghavi-Helm et al., 2014; Jin et al., 2013; Pan et al., 2008; Stavreva et al., 2015) have not provided a clear consensus on the plasticity of chromatin loops. Here we have used the newly developed PCHi-C (Schoenfelder et al., 2015) to assess looping plasticity during differentiation of 3T3-L1 preadipocytes. We demonstrate that the promoter-anchored chromatin loops are rapidly reorganized in response to the differentiation cocktail (Figure 7E), which is particularly striking considering that these cells are already committed to become adipocytes. Thus, in contrast to the preprogramming of chromatin loops described previously (Ghavi-Helm et al., 2014; Jin et al., 2013), this indicates that many promoter-anchored chromatin loops are not hard-wired in the genome of a given cell type, but rather respond in a highly dynamic manner to external stimuli. Importantly, we demonstrate that these dynamic chromatin loops are coupled with dynamic regulation of gene expression and enhancer activity. This indicates that dynamic rewiring of promoter-enhancer loops is an important general mechanism linking reprogramming of enhancer activity to changes in target gene expression. This is consistent with a recent elegant study demonstrating that forced looping of enhancers to promoters induces gene activation (Bartman et al., 2016) as well as the finding from the present study that allele-selective promoter-anchored chromatin loops are associated with allele-selective gene expression from the connected promoters.

In general, during the first 4 hours of differentiation we did not observe dramatic changes in H3K4me1 and -2 levels at promoter-anchored enhancers in response to adipogenic inducers, whereas H3K27ac is highly dynamic at these regions. Thus, acute enhancer activation in response to adipogenic inducers appears to involve deposition of H3K27ac at already poised enhancers (i.e., regions pre-marked by H3K4me1) rather than de novo establishment of enhancers. This is in line with the reported

(C) Bars indicate the fraction of dynamic interactions marked by the indicated epigenomic marks or bound by the indicated coregulators, where the ChIP-seq signal is constant (gray) or the ChIP-seq and PCHi-C signal change in the same direction (equidirectional, green) or in opposite directions (antidirectional, brown). The number of analyzed interactions is indicated above each bar.

(D) Left, the average ChIP-seq signal around super-enhancers that are significantly induced at 4 hr is shown as a line plot. The super-enhancers have been adjusted to the same size. Input is included as a control. Right, the distributions of the signals within these super-enhancers are shown as boxplots. Related to Figure S4.

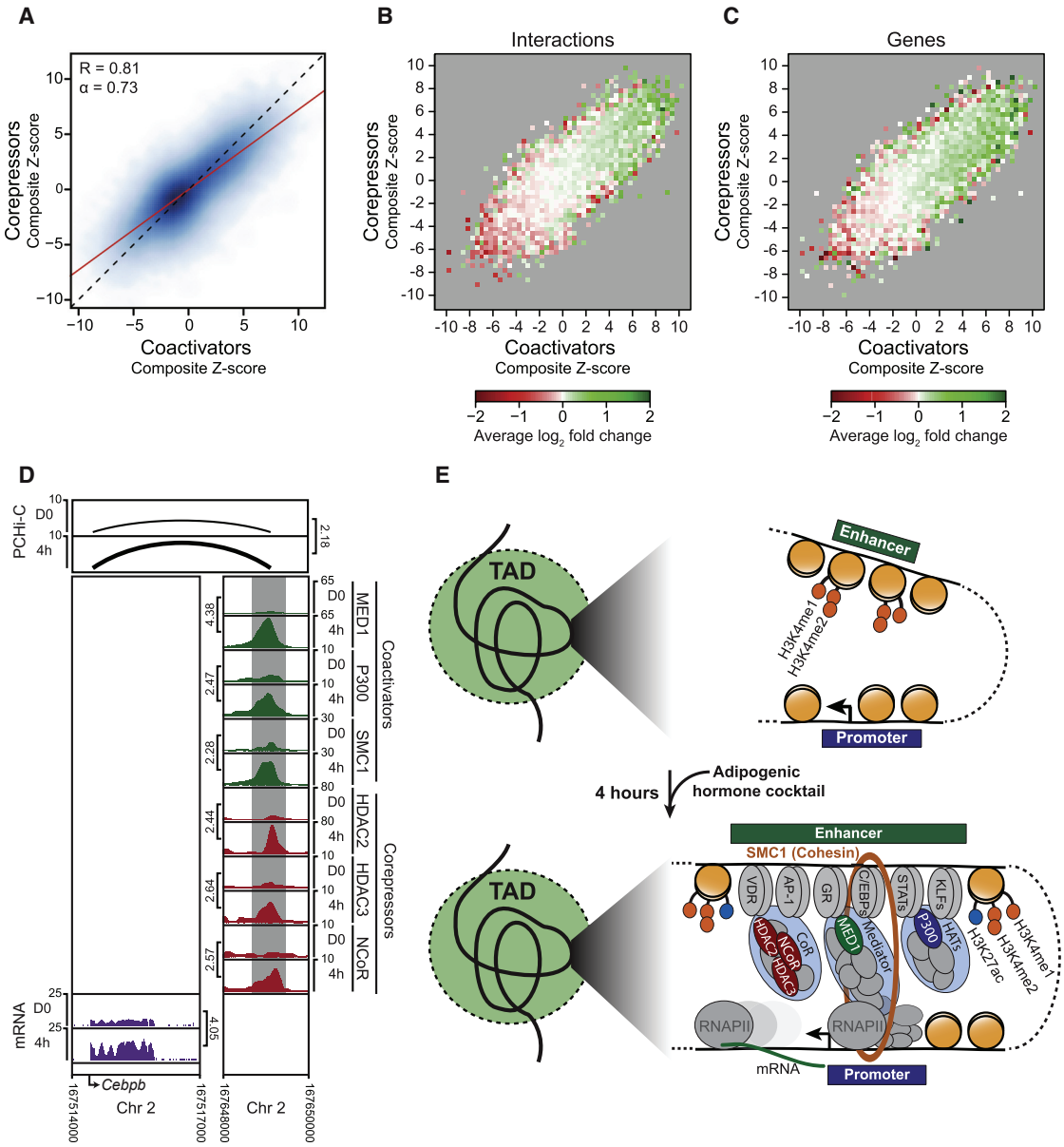

Figure 7. Corepressors Are Recruited to Activated Enhancers that Control Gene Activation through Chromatin Loop Formation

(A) A composite score of changes in corepressor and coactivator binding was constructed by combining Z-transformed changes in ChIP-seq binding for three corepressors (i.e., HDAC2, -3, and NCoR) and three coactivators (i.e., MED1, SMC1, and P300), respectively (see STAR Methods for more details). The changes in this combined measure of corepressor and coactivator binding during the first 4 hr of differentiation were visualized in a smooth scatterplot (see Figure S6B for pairwise comparison of all corepressors and coactivators individually). The slope (α) and the Pearson correlation (R) are shown. All regions identified as a binding site for at least one coregulator on at least one time point are included in the analyses.

(B and C) The scatterplot from (A) was subdivided into bins that were colored according to the mean fold change of the promoter-anchored interactions associated with the corepressor/coactivator binding sites in each bin (B) or the mean fold change of the expression of the genes connected to the corepressor/coactivator binding sites through chromatin loops (C). Only coregulator binding sites involved in promoter-anchored chromatin loops are shown.

(D) WashU screenshot of *Cebpb* and a connected enhancer. Binding of corepressors and coactivators to the enhancer as determined by ChIP-seq (bottom right), promoter-enhancer chromatin loop formation as determined by PCHi-C (top), and *Cebpb* expression as determined by mRNA-seq (bottom left) in preadipocytes (i.e., prior to induction of differentiation) and 4 hr after stimulation with the adipogenic hormone cocktail are shown. The height of the loop as well as the thickness of the loop line indicates the strength of the promoter-enhancer interaction (top). Fold changes for interaction strength, corepressor/coactivator binding, and expression level are indicated in vertical orientation.

(E) Proposed model of the mechanism controlling enhancer reprogramming and 3D reorganization during adipocyte differentiation. Related to Figures S5–S7.

mechanism of enhancer activation during differentiation of ESCs (Creyghton et al., 2010; Rada-Iglesias et al., 2011). Importantly, we found that dynamic rewiring of promoter-enhancer loops is linked to dynamic changes in H3K27ac, but not H3K4me1 and -2. This is in striking contrast to the highly predictive value of H3K4me1 for differential looping in ESCs compared to more differentiated progenitor cell types (Dixon et al., 2015). Thus, it appears that H3K4me1 and -2 may prime enhancers for interaction with target promoters but that other marks, such as H3K27Ac, are more closely linked to dynamic modulation of promoter-enhancer loops.

It should be noted that many of the identified interactions connect promoters and distal genomic regions that do not appear to be marked by the known enhancer-associated coregulators investigated here (i.e., MED1, SMC1, and P300), consistent with recently reported findings (Cairns et al., 2016; Javierre et al., 2016; Jin et al., 2013; Sanyal et al., 2012; Schoenfelder et al., 2015). Although it cannot be excluded that some of these interactions are false positives, this indicates that promoter-anchored chromatin loops may form independently of these factors. Future studies to identify additional factors and marks controlling promoter-anchored interactions will be of great interest.

Corepressors are usually associated with transcriptional repression, e.g., by modulating the epigenomic landscape to produce a repressive chromatin signature. In contrast to this dogma, we demonstrate that recruitment of the well-known corepressors HDAC2, -3, and NCoR in preadipocytes in response to adipogenic inducers is associated with enhancer activation, the establishment of promoter-enhancer chromatin loops, and gene activation (Figure 7E). Conversely, transcriptional repression in early 3T3-L1 differentiation is mainly associated with decommissioning of enhancers. These findings indicate that corepressors such as NCoR and HDACs may play a previously unrecognized role at enhancers during transcriptional activation. In line with this, we have previously demonstrated that several corepressors, including HDAC1 and -2 as well as NCoR and SMRT, co-immunoprecipitate with C/EBPβ (Siersbæk et al., 2014), which plays a key role in transcriptional activation during early adipocyte differentiation (Siersbæk et al., 2012). Based on the striking correlation between the binding of both corepressors and coactivators with that of pro-adipogenic transcription factors, we propose a mechanism where pro-adipogenic transcription factors are involved in recruiting both corepressors and coactivators to activated enhancers (Figure 7E). These findings are in striking contrast to a previous report on the role of SMRT during 3T3-L1 differentiation, which showed that SMRT binding is high in preadipocytes and that loss of SMRT upon induction of differentiation is associated with gene activation (Raghav et al., 2012). The reason for this discrepancy is currently unclear, but it clearly warrants further mechanistic studies on the role of corepressors at enhancer regions.

The finding that corepressors are recruited to activated enhancers that engage in activating promoter-enhancer loops begs the question of what their functional role is at these regulatory regions. The most obvious hypothesis is that the corepressors function as molecular brakes that prevent "over-activation" of enhancers and target genes, consistent with the proposed role of HDACs at promoters (Wang et al., 2009). Alternatively, recruitment of corepressors may be functionally important for establishment of some active enhancers as has been described previously for selected enhancers (Adikesavan et al., 2014; Peterson et al., 2007).

In conclusion, we demonstrate a rapid rewiring of promoter-anchored chromatin loops in response to adipogenic hormones. This 3D reorganization of the chromatin is coupled to changes in gene expression as well as dramatic reprogramming of (super-) enhancer activity, which includes changes in H3K27ac, but not H3K4me1 and -2 marks. Furthermore, our data show that activation of adipogenic enhancers is associated with extensive recruitment of corepressors as well as coactivators.

STAR★METHODS

Detailed methods are provided in the online version of this paper and include the following:

- KEY RESOURCES TABLE
- CONTACT FOR REAGENT AND RESOURCE SHARING
- EXPERIMENTAL MODEL AND SUBJECT DETAILS
  - Cell lines
- METHOD DETAILS
  - Crosslinking of cells for Hi-C and PCHi-C
  - Hi-C library preparation
  - Biotinylated RNA bait library design
  - PCHi-C
  - Hi-C and PCHi-C Sequencing
  - Hi-C and PCHi-C sequence alignment
  - ChIP-seq
  - mRNA-seq
- QUANTIFICATION AND STATISTICAL ANALYSIS
  - Topological associating domains (TADs)
  - HSV transformation of PCHi-C data
  - mRNA-seq analyses
  - ChIP-seq analyses
  - Calling super-enhancers based on MED1 ChIP-seq data
  - Calculating enrichment/depletion of interactions at enhancers and gene promoters
  - Prediction of dynamic chromatin loops
  - Composite corepressor and coactivator scores
  - Allele-specificity of interactions
  - eQTL analysis
- DATA AND SOFTWARE AVAILABILITY
  - Data availability
  - Code availability

SUPPLEMENTAL INFORMATION

Supplemental Information includes seven figures and one table and can be found with this article online at http://dx.doi.org/10.1016/j.molcel.2017.04.010.

AUTHOR CONTRIBUTIONS

Conceptualization, R.S., S.M., and P.F; Investigation, R.S., B.M.J., R.N., E.K.B., and S.T.; Formal Analysis, J.G.S.M., J.C., S.W.W., and R.S.; Visualization, J.G.S.M. and R.S.; Writing – Original Draft, R.S. and S.M.; Writing – Review

& Editing, R.S., J.G.S.M., B.M.J., R.N., J.C., M.S., P.F., and S.M.; Supervision, S.M., P.F., and M.S.; Project Administration, R.S. and S.M.; Funding Acquisition, S.M., P.F., and M.S.

ACKNOWLEDGMENTS

We thank members of the Mandrup, Fraser, and Spivakov groups for fruitful discussions. This work was mainly carried out at the Villum Center for Bioanalytical Sciences, Department of Biochemistry and Molecular Biology, SDU, supported by the Villum Foundation. Work in the Mandrup laboratory was supported by grants from the Danish Independent Research Council | Natural Sciences (12-125524), the Danish Diabetes Academy supported by Novo Nordisk Foundation, the Lundbeck Foundation (R118-A11639), and the Augustinus Foundation. R.S. is currently funded by a fellowship from the Novo Nordisk Foundation (NNF15OC0014136). Work in the Fraser and Spivakov groups were supported by the Medical Research Council, UK, MR/L007150/1 and Biotechnology and Biological Research Council, UK, BB/J004480/1.

Received: December 13, 2016
Revised: March 6, 2017
Accepted: April 11, 2017
Published: May 4, 2017

REFERENCES

Adikesavan, A.K., Karmakar, S., Pardo, P., Wang, L., Liu, S., Li, W., and Smith, C.L. (2014). Activation of p53 transcriptional activity by SMRT: a histone deacetylase 3-independent function of a transcriptional corepressor. Mol. Cell. Biol. *34*, 1246–1261.

Bartman, C.R., Hsu, S.C., Hsiung, C.C., Raj, A., and Blobel, G.A. (2016). Enhancer Regulation of Transcriptional Bursting Parameters Revealed by Forced Chromatin Looping. Mol. Cell *62*, 237–247.

Battulin, N., Fishman, V.S., Mazur, A.M., Pomaznoy, M., Khabarova, A.A., Afonnikov, D.A., Prokhortchouk, E.B., and Serov, O.L. (2015). Comparison of the three-dimensional organization of sperm and fibroblast genomes using the Hi-C approach. Genome Biol. *16*, 77.

Bernlohr, D.A., Angus, C.W., Lane, M.D., Bolanowski, M.A., and Kelly, T.J., Jr. (1984). Expression of specific mRNAs during adipose differentiation: identification of an mRNA encoding a homologue of myelin P2 protein. Proc. Natl. Acad. Sci. USA *81*, 5468–5472.

Cairns, J., Freire-Pritchett, P., Wingett, S.W., Várnai, C., Dimond, A., Plagnol, V., Zerbino, D., Schoenfelder, S., Javierre, B.M., Osborne, C., et al. (2016). CHiCAGO: robust detection of DNA looping interactions in Capture Hi-C data. Genome Biol. *17*, 127.

Consortium, E.P., Dunham, I., Kundaje, A., Aldred, S., Collins, P., Davis, C., Doyle, F., Epstein, C., Frietze, S., Harrow, J., et al.; ENCODE Project Consortium (2012). An integrated encyclopedia of DNA elements in the human genome. Nature *489*, 57–74.

Creyghton, M.P., Cheng, A.W., Welstead, G.G., Kooistra, T., Carey, B.W., Steine, E.J., Hanna, J., Lodato, M.A., Frampton, G.M., Sharp, P.A., et al. (2010). Histone H3K27ac separates active from poised enhancers and predicts developmental state. Proc. Natl. Acad. Sci. USA *107*, 21931–21936.

Dixon, J.R., Selvaraj, S., Yue, F., Kim, A., Li, Y., Shen, Y., Hu, M., Liu, J.S., and Ren, B. (2012). Topological domains in mammalian genomes identified by analysis of chromatin interactions. Nature *485*, 376–380.

Dixon, J.R., Jung, I., Selvaraj, S., Shen, Y., Antosiewicz-Bourget, J.E., Lee, A.Y., Ye, Z., Kim, A., Rajagopal, N., Xie, W., et al. (2015). Chromatin architecture reorganization during stem cell differentiation. Nature *518*, 331–336.

Dobin, A., Davis, C.A., Schlesinger, F., Drenkow, J., Zaleski, C., Jha, S., Batut, P., Chaisson, M., and Gingeras, T.R. (2013). STAR: ultrafast universal RNA-seq aligner. Bioinformatics *29*, 15–21.

Dowen, J.M., Fan, Z.P., Hnisz, D., Ren, G., Abraham, B.J., Zhang, L.N., Weintraub, A.S., Schuijers, J., Lee, T.I., Zhao, K., and Young, R.A. (2014). Control of cell identity genes occurs in insulated neighborhoods in mammalian chromosomes. Cell *159*, 374–387.

Fullwood, M.J., Liu, M.H., Pan, Y.F., Liu, J., Xu, H., Mohamed, Y.B., Orlov, Y.L., Velkov, S., Ho, A., Mei, P.H., et al. (2009). An oestrogen-receptor-alpha-bound human chromatin interactome. Nature *462*, 58–64.

Ghavi-Helm, Y., Klein, F.A., Pakozdi, T., Ciglar, L., Noordermeer, D., Huber, W., and Furlong, E.E. (2014). Enhancer loops appear stable during development and are associated with paused polymerase. Nature *512*, 96–100.

Graves, R.A., Tontonoz, P., Ross, S.R., and Spiegelman, B.M. (1991). Identification of a potent adipocyte-specific enhancer: involvement of an NF-1-like factor. Genes Dev. *5*, 428–437.

Hasin-Brumshtein, Y., Khan, A.H., Hormozdiari, F., Pan, C., Parks, B.W., Petyuk, V.A., Piehowski, P.D., Brümmer, A., Pellegrini, M., Xiao, X., et al. (2016). Hypothalamic transcriptomes of 99 mouse strains reveal trans eQTL hotspots, splicing QTLs and novel non-coding genes. eLife *5*, 5.

Heidari, N., Phanstiel, D.H., He, C., Grubert, F., Jahanbani, F., Kasowski, M., Zhang, M.Q., and Snyder, M.P. (2014). Genome-wide map of regulatory interactions in the human genome. Genome Res. *24*, 1905–1917.

Heinz, S., Benner, C., Spann, N., Bertolino, E., Lin, Y.C., Laslo, P., Cheng, J.X., Murre, C., Singh, H., and Glass, C.K. (2010). Simple combinations of lineage-determining transcription factors prime cis-regulatory elements required for macrophage and B cell identities. Mol. Cell *38*, 576–589.

Ing-Simmons, E., Seitan, V.C., Faure, A.J., Flicek, P., Carroll, T., Dekker, J., Fisher, A.G., Lenhard, B., and Merkenschlager, M. (2015). Spatial enhancer clustering and regulation of enhancer-proximal genes by cohesin. Genome Res. *25*, 504–513.

Javierre, B.M., Burren, O.S., Wilder, S.P., Kreuzhuber, R., Hill, S.M., Sewitz, S., Cairns, J., Wingett, S.W., Várnai, C., Thiecke, M.J., et al.; BLUEPRINT Consortium (2016). Lineage-Specific Genome Architecture Links Enhancers and Non-coding Disease Variants to Target Gene Promoters. Cell *167*, 1369–1384.e19.

Ji, X., Dadon, D.B., Powell, B.E., Fan, Z.P., Borges-Rivera, D., Shachar, S., Weintraub, A.S., Hnisz, D., Pegoraro, G., Lee, T.I., et al. (2016). 3D Chromosome Regulatory Landscape of Human Pluripotent Cells. Cell Stem Cell *18*, 262–275.

Jin, F., Li, Y., Dixon, J.R., Selvaraj, S., Ye, Z., Lee, A.Y., Yen, C.A., Schmitt, A.D., Espinoza, C.A., and Ren, B. (2013). A high-resolution map of the three-dimensional chromatin interactome in human cells. Nature *503*, 290–294.

Kagey, M.H., Newman, J.J., Bilodeau, S., Zhan, Y., Orlando, D.A., van Berkum, N.L., Ebmeier, C.C., Goossens, J., Rahl, P.B., Levine, S.S., et al. (2010). Mediator and cohesin connect gene expression and chromatin architecture. Nature *467*, 430–435.

Krijger, P.H., Di Stefano, B., de Wit, E., Limone, F., van Oevelen, C., de Laat, W., and Graf, T. (2016). Cell-of-Origin-Specific 3D Genome Structure Acquired during Somatic Cell Reprogramming. Cell Stem Cell *18*, 597–610.

Li, G., Ruan, X., Auerbach, R.K., Sandhu, K.S., Zheng, M., Wang, P., Poh, H.M., Goh, Y., Lim, J., Zhang, J., et al. (2012). Extensive promoter-centered chromatin interactions provide a topological basis for transcription regulation. Cell *148*, 84–98.

Li, L., Lyu, X., Hou, C., Takenaka, N., Nguyen, H.Q., Ong, C.T., Cubeñas-Potts, C., Hu, M., Lei, E.P., Bosco, G., et al. (2015). Widespread rearrangement of 3D chromatin organization underlies polycomb-mediated stress-induced silencing. Mol. Cell *58*, 216–231.

Lieberman-Aiden, E., van Berkum, N.L., Williams, L., Imakaev, M., Ragoczy, T., Telling, A., Amit, I., Lajoie, B.R., Sabo, P.J., Dorschner, M.O., et al. (2009). Comprehensive mapping of long-range interactions reveals folding principles of the human genome. Science *326*, 289–293.

Love, M.I., Huber, W., and Anders, S. (2014). Moderated estimation of fold change and dispersion for RNA-seq data with DESeq2. Genome Biol. *15*, 550.

Lovén, J., Hoke, H.A., Lin, C.Y., Lau, A., Orlando, D.A., Vakoc, C.R., Bradner, J.E., Lee, T.I., and Young, R.A. (2013). Selective inhibition of tumor oncogenes by disruption of super-enhancers. Cell *153*, 320–334.

Lupiáñez, D.G., Kraft, K., Heinrich, V., Krawitz, P., Brancati, F., Klopocki, E., Horn, D., Kayserili, H., Opitz, J.M., Laxova, R., et al. (2015). Disruptions of topological chromatin domains cause pathogenic rewiring of gene-enhancer interactions. Cell *161*, 1012–1025.

Malik, S., and Roeder, R.G. (2010). The metazoan Mediator co-activator complex as an integrative hub for transcriptional regulation. Nat. Rev. Genet. *11*, 761–772.

Maurano, M.T., Humbert, R., Rynes, E., Thurman, R.E., Haugen, E., Wang, H., Reynolds, A.P., Sandstrom, R., Qu, H., Brody, J., et al. (2012). Systematic localization of common disease-associated variation in regulatory DNA. Science *337*, 1190–1195.

Mikkelsen, T.S., Xu, Z., Zhang, X., Wang, L., Gimble, J.M., Lander, E.S., and Rosen, E.D. (2010). Comparative epigenomic analysis of murine and human adipogenesis. Cell *143*, 156–169.

Nagano, T., Várnai, C., Schoenfelder, S., Javierre, B.M., Wingett, S.W., and Fraser, P. (2015). Comparison of Hi-C results using in-solution versus in-nucleus ligation. Genome Biol. *16*, 175.

Nielsen, R., and Mandrup, S. (2014). Genome-wide profiling of transcription factor binding and epigenetic marks in adipocytes by ChIP-seq. Methods Enzymol. *537*, 261–279.

Nora, E.P., Lajoie, B.R., Schulz, E.G., Giorgetti, L., Okamoto, I., Servant, N., Piolot, T., van Berkum, N.L., Meisig, J., Sedat, J., et al. (2012). Spatial partitioning of the regulatory landscape of the X-inactivation centre. Nature *485*, 381–385.

Pan, Y.F., Wansa, K.D., Liu, M.H., Zhao, B., Hong, S.Z., Tan, P.Y., Lim, K.S., Bourque, G., Liu, E.T., and Cheung, E. (2008). Regulation of estrogen receptor-mediated long range transcription via evolutionarily conserved distal response elements. J. Biol. Chem. *283*, 32977–32988.

Park, K.W., Waki, H., Villanueva, C.J., Monticelli, L.A., Hong, C., Kang, S., MacDougald, O.A., Goldrath, A.W., and Tontonoz, P. (2008). Inhibitor of DNA binding 2 is a small molecule-inducible modulator of peroxisome proliferator-activated receptor-γ expression and adipocyte differentiation. Mol. Endocrinol. *22*, 2038–2048.

Peterson, T.J., Karmakar, S., Pace, M.C., Gao, T., and Smith, C.L. (2007). The silencing mediator of retinoic acid and thyroid hormone receptor (SMRT) corepressor is required for full estrogen receptor alpha transcriptional activity. Mol. Cell. Biol. *27*, 5933–5948.

Phillips-Cremins, J.E., Sauria, M.E., Sanyal, A., Gerasimova, T.I., Lajoie, B.R., Bell, J.S., Ong, C.T., Hookway, T.A., Guo, C., Sun, Y., et al. (2013). Architectural protein subclasses shape 3D organization of genomes during lineage commitment. Cell *153*, 1281–1295.

Quinlan, A.R., and Hall, I.M. (2010). BEDTools: a flexible suite of utilities for comparing genomic features. Bioinformatics *26*, 841–842.

R Core Team (2013). R: A language and environment for statistical computing (R Foundation for Statistical Computing).

Rada-Iglesias, A., Bajpai, R., Swigut, T., Brugmann, S.A., Flynn, R.A., and Wysocka, J. (2011). A unique chromatin signature uncovers early developmental enhancers in humans. Nature *470*, 279–283.

Raghav, S.K., Waszak, S.M., Krier, I., Gubelmann, C., Isakova, A., Mikkelsen, T.S., and Deplancke, B. (2012). Integrative genomics identifies the corepressor SMRT as a gatekeeper of adipogenesis through the transcription factors C/EBPβ and KAISO. Mol. Cell *46*, 335–350.

Rimmer, A., Phan, H., Mathieson, I., Iqbal, Z., Twigg, S.R.F., Wilkie, A.O., McVean, G., and Lunter, G.; WGS500 Consortium (2014). Integrating mapping-, assembly- and haplotype-based approaches for calling variants in clinical sequencing applications. Nat. Genet. *46*, 912–918.

Robin, X., Turck, N., Hainard, A., Tiberti, N., Lisacek, F., Sanchez, J.C., and Müller, M. (2011). pROC: an open-source package for R and S+ to analyze and compare ROC curves. BMC Bioinformatics *12*, 77.

Robinson, M.D., McCarthy, D.J., and Smyth, G.K. (2010). edgeR: a Bioconductor package for differential expression analysis of digital gene expression data. Bioinformatics *26*, 139–140.

Sahlén, P., Abdullayev, I., Ramsköld, D., Matskova, L., Rilakovic, N., Lötstedt, B., Albert, T.J., Lundeberg, J., and Sandberg, R. (2015). Genome-wide mapping of promoter-anchored interactions with close to single-enhancer resolution. Genome Biol. *16*, 156.

Sanyal, A., Lajoie, B.R., Jain, G., and Dekker, J. (2012). The long-range interaction landscape of gene promoters. Nature *489*, 109–113.

Schoenfelder, S., Furlan-Magaril, M., Mifsud, B., Tavares-Cadete, F., Sugar, R., Javierre, B.M., Nagano, T., Katsman, Y., Sakthidevi, M., Wingett, S.W., et al. (2015). The pluripotent regulatory circuitry connecting promoters to their long-range interacting elements. Genome Res. *25*, 582–597.

Siersbæk, R., and Mandrup, S. (2011). Transcriptional networks controlling adipocyte differentiation. Cold Spring Harb. Symp. Quant. Biol. *76*, 247–255.

Siersbæk, R., Nielsen, R., John, S., Sung, M.-H., Baek, S., Loft, A., Hager, G.L., and Mandrup, S. (2011). Extensive chromatin remodelling and establishment of transcription factor 'hotspots' during early adipogenesis. EMBO J. *30*, 1459–1472.

Siersbæk, R., Nielsen, R., and Mandrup, S. (2012). Transcriptional networks and chromatin remodeling controlling adipogenesis. Trends Endocrinol. Metab. *23*, 56–64.

Siersbæk, R., Rabiee, A., Nielsen, R., Sidoli, S., Traynor, S., Loft, A., La Cour Poulsen, L., Rogowska-Wrzesinska, A., Jensen, O.N., and Mandrup, S. (2014). Transcription factor cooperativity in early adipogenic hotspots and super-enhancers. Cell Rep. *7*, 1443–1455.

Stavreva, D.A., Coulon, A., Baek, S., Sung, M.H., John, S., Stixova, L., Tesikova, M., Hakim, O., Miranda, T., Hawkins, M., et al. (2015). Dynamics of chromatin accessibility and long-range interactions in response to glucocorticoid pulsing. Genome Res. *25*, 845–857.

Steger, D.J., Grant, G.R., Schupp, M., Tomaru, T., Lefterova, M.I., Schug, J., Manduchi, E., Stoeckert, C.J., Jr., and Lazar, M.A. (2010). Propagation of adipogenic signals through an epigenomic transition state. Genes Dev. *24*, 1035–1044.

Step, S.E., Lim, H.W., Marinis, J.M., Prokesch, A., Steger, D.J., You, S.H., Won, K.J., and Lazar, M.A. (2014). Anti-diabetic rosiglitazone remodels the adipocyte transcriptome by redistributing transcription to PPARγ-driven enhancers. Genes Dev. *28*, 1018–1028.

Thurman, R.E., Rynes, E., Humbert, R., Vierstra, J., Maurano, M.T., Haugen, E., Sheffield, N.C., Stergachis, A.B., Wang, H., Vernot, B., et al. (2012). The accessible chromatin landscape of the human genome. Nature *489*, 75–82.

van de Geijn, B., McVicker, G., Gilad, Y., and Pritchard, J.K. (2015). WASP: allele-specific software for robust molecular quantitative trait locus discovery. Nat. Methods *12*, 1061–1063.

Wang, Z., Zang, C., Cui, K., Schones, D.E., Barski, A., Peng, W., and Zhao, K. (2009). Genome-wide mapping of HATs and HDACs reveals distinct functions in active and inactive genes. Cell *138*, 1019–1031.

Watson, P.J., Fairall, L., and Schwabe, J.W. (2012). Nuclear hormone receptor co-repressors: structure and function. Mol. Cell. Endocrinol. *348*, 440–449.

Whyte, W.A., Orlando, D.A., Hnisz, D., Abraham, B.J., Lin, C.Y., Kagey, M.H., Rahl, P.B., Lee, T.I., and Young, R.A. (2013). Master transcription factors and mediator establish super-enhancers at key cell identity genes. Cell *153*, 307–319.

Wingett, S., Ewels, P., Furlan-Magaril, M., Nagano, T., Schoenfelder, S., Fraser, P., and Andrews, S. (2015). HiCUP: pipeline for mapping and processing Hi-C data. F1000Res. *4*, 1310.

Yan, J., Enge, M., Whitington, T., Dave, K., Liu, J., Sur, I., Schmierer, B., Jolma, A., Kivioja, T., Taipale, M., and Taipale, J. (2013). Transcription factor binding in human cells occurs in dense clusters formed around cohesin anchor sites. Cell *154*, 801–813.

Zuin, J., Dixon, J.R., van der Reijden, M.I., Ye, Z., Kolovos, P., Brouwer, R.W., van de Corput, M.P., van de Werken, H.J., Knoch, T.A., van IJcken, W.F., et al. (2014). Cohesin and CTCF differentially affect chromatin architecture and gene expression in human cells. Proc. Natl. Acad. Sci. USA *111*, 996–1001.

STAR★METHODS

KEY RESOURCES TABLE

REAGENT or RESOURCE	SOURCE	IDENTIFIER
Antibodies		
Rabbit polyclonal MED1/TRAP220 antibody (M-255)	Santa Cruz	Cat#sc-8998; RRID: AB_2144021
Rabbit polyclonal SMC1 antibody	Bethyl Laboratories	Cat#A300-055A; RRID: AB_2192467
Rabbit polyclonal CTCF antibody	Millipore	Cat#07-729; RRID: AB_441965
Rabbit polyclonal P300 antibody (N-15)	Santa Cruz	Cat#sc-584; RRID: AB_2293429
Rabbit polyclonal HDAC2 antibody	Bethyl Laboratories	Cat#A300-705A; RRID: AB_533399
Rabbit polyclonal HDAC3 antibody (H-99)	Santa Cruz	Cat#sc-11417; RRID: AB_2118706
Rabbit polyclonal NCoR antibody	Bethyl Laboratories	Cat#A301-145A; RRID: AB_873085
Rabbit polyclonal H3K27ac antibody	Abcam	Cat#ab4729; RRID: AB_2118291
Rabbit polyclonal H3K4me1 antibody	Abcam	Cat#ab8895; RRID: AB_306847
Rabbit polyclonal H3K4me2 antibody	Cell Signaling	Cat#9726; RRID: AB_915839
Chemicals, Peptides, and Recombinant Proteins		
Insulin	Sigma-Aldrich	I9278
Dexamethasone	Sigma-Aldrich	D4902
3-Isobutyl-1-methylxanthine	Sigma-Aldrich	I5879
Critical Commercial Assays		
TruSeq Illumina mRNA prep kit	Illumina	RS-122-2001
HiSeq v4 Illumina SR sequencing kit (mRNaseq/ChIPseq)	Illumina	GD-401-4001 FC-401-4002
NEB ChIPseq prep kit	Nielsen and Mandrup, 2014	Section 2.3
HiSeq v4 Illumina PE sequencing kit (for HiC and PCHiC)	Illumina	PE-401-4001 FC-401-4002
Quant-iT PicoGreen dsDNA Assay Kit	Thermo Fisher	Cat#P7589
SureSelectXT Custom 3-5.9Mb library	Agilent Technologies	5190-4831
SSEL TE Reagement Kit, ILM PE full adaptor	Agilent Technologies	Cat#931108
Deposited Data		
Raw and analyzed data	This paper	GEO: GSE95533
Experimental Models: Cell Lines		
3T3-L1	ATCC	Cat#CL-173; RRID:CVCL_0123
Software and Algorithms		
HOMER	Heinz et al., 2010	http://homer.ucsd.edu/homer/
Bedtools	Quinlan and Hall, 2010	http://bedtools.readthedocs.io/en/latest/
ROSE package	Lovén et al., 2013; Whyte et al., 2013	http://younglab.wi.mit.edu/super_enhancer_code.html
STAR aligner	Dobin et al., 2013	https://github.com/alexdobin/STAR
DEseq2	Love et al., 2014	https://bioconductor.org/packages/release/bioc/html/DESeq2.html
HiCUP	Wingett et al., 2015	http://www.bioinformatics.babraham.ac.uk/projects/hicup
CHiCAGO	Cairns et al., 2016	http://regulatorygenomicsgroup.org/chicago
edgeR	Robinson et al., 2010	https://bioconductor.org/packages/release/bioc/html/edgeR.html
WASP	van de Geijn et al., 2015	https://github.com/bmvdgeijn/WASP/
Platypus	Rimmer et al., 2014	http://www.well.ox.ac.uk/platypus

CONTACT FOR REAGENT AND RESOURCE SHARING

Further information and requests for resources and reagents should be directed to and will be fulfilled by the Lead Contact, Susanne Mandrup (s.mandrup@bmb.sdu.dk).

EXPERIMENTAL MODEL AND SUBJECT DETAILS

Cell lines

Mouse 3T3-L1 cells (obtained from ATCC) were grown in Dulbecco's Modified Eagle's Medium (DMEM, #52-100-021, GIBCO) supplemented with 10% calf serum (#B15-005, PAA) and 1% pen/strep (#DE 17-602E, Lonza). Cells were induced to differentiate two days post confluency by addition of differentiation media (DMEM supplemented with 10% fetal bovine serum (#S 01 15, Biochrom) and 1% pen/strep) supplemented with 1 μg/ml insulin (Sigma-Aldrich, I9278), 390 ng/ml dexamethasone (Sigma-Aldrich, D4902) and 1115 μg/ml 3-Isobutyl-1-methylxanthine (Sigma-Aldrich, I5879). Two days after induction of differentiation, fresh differentiation media supplemented with 1 μg/ml insulin were added. From day four and onward, differentiated cells were maintained in differentiation media.

METHOD DETAILS

Crosslinking of cells for Hi-C and PCHi-C

Two biological replicates of approximately 50-80 millions of 3T3-L1 cells were crosslinked for 10 min by 2% formaldehyde in PBS at different time points during the first two days of differentiation (day 0 (before stimulation with the adipogenic cocktail), 4 hr, and day 2). Crosslinking was quenched by addition of 0.125M glycine. Cells were incubated at room temperature for 5 min and then on ice for 15 min. Crosslinked cells were washed once in cold PBS, and the cell pellets were flash frozen in liquid nitrogen and stored at −80°C.

Hi-C library preparation

Hi-C library generation was carried out with in-nucleus ligation as described previously (Nagano et al., 2015). Briefly, chromatin was digested over night by HindIII enzyme in NEBuffer 2. Digested ends were filled in using biotinylated d-ATP and ligated in preserved nuclei. Chromatin was then de-crosslinked and purified by phenol-chloroform extraction. DNA concentration was measured using Quant-iT PicoGreen (Life Technologies), and 50 μg of DNA was sheared to an average size of 400 bp, using the manufacturer's instructions (Covaris). The sheared DNA was end-repaired, adenine-tailed and double size-selected using AMPure XP beads to isolate DNA ranging from 250 to 550 bp. Ligation fragments marked by biotin were immobilized using MyOne Streptavidin C1 DynaBeads (Invitrogen) and ligated to paired-end adaptors (Illumina). The immobilized Hi-C libraries were amplified using PE PCR 1.0 and PE PCR 2.0 primers (Illumina) with 7–8 PCR amplification cycles.

Biotinylated RNA bait library design

39,021 biotinylated 120-mer RNA baits were designed to the ends of HindIII restriction fragments that overlap 25,747 Ensembl-annotated promoters of protein-coding, noncoding, antisense, snRNA, miRNA and snoRNA transcripts (Schoenfelder et al., 2015). A target sequence was accepted if its GC content ranged between 25% and 65%, the sequence contained no more than two consecutive Ns and was within 330 bp of the HindIII restriction fragment terminus.

PCHi-C

Capture Hi-C of promoters was carried out with SureSelect target enrichment (SureSelectXT Custom 3-5.9Mb library described above), using the custom-designed biotinylated RNA bait library and custom paired-end blockers according to the manufacturer's instructions (Agilent Technologies). Between 500 ng to 1 μg of Hi-C library were captured. After library enrichment, a post-capture PCR amplification step was carried out using PE PCR 1.0 and PE PCR 2.0 primers with 4 PCR amplification cycles.

Hi-C and PCHi-C Sequencing

Hi-C and PCHi-C libraries were sequenced on the Illumina HiSeq2500 platform using HiSeq v4 Illumina PE sequencing kit according to the manufacturer's instructions. Different sequencing lanes per PCHi-C library and per Hi-C library were used in order to obtain similar number of valid reads.

Hi-C and PCHi-C sequence alignment

Raw sequencing reads were processed using the HiCUP pipeline (Wingett et al., 2015), which maps the positions of di-tags against the mouse genome (NCBIM37), filters out experimental artifacts, such as circularized reads and re-ligations, and removes all duplicate reads. See Table S1 for an overview of Hi-C and PCHi-C sequencing depth.

ChIP-seq

Chromatin immunoprecipitation combined with deep sequencing (ChIP-seq) was performed essentially as described previously (Nielsen and Mandrup, 2014). Two biological replicates (i.e., different differentiations) were done for each factor.

Crosslinking

For MED1/TRAP220, SMC1, P300, HDAC2, HDAC3 and NCoR ChIP-seq: Cells were crosslinked by 2 mM disuccinimidyl glutarate (DSG) for 20-30 min at RT followed by 1% formaldehyde for 10 min at RT. Crosslinking was quenched by addition of 0.125M glycine for 10 min. For CTCF and histone mark ChIP-seq: Cells were crosslinked in formaldehyde only as described above.

Sonication and immunoprecipitation

For MED1/TRAP220, SMC1, CTCF and histone marks: Crosslinked cells were scraped in ChIP lysis buffer (0.1% SDS, 1% Triton X-100, 0.15M NaCl, 1mM EDTA, 20mM Tris, pH = 8) and sonicated for 40 cycles (approximately 10-12 million crosslinked cells in 1.5 mL lysis buffer was sonicated in 15 mL tubes, 30 s on, 30 s off, maximum intensity) in a Bioruptor (Diagenode). For P300, HDAC2, HDAC3 and NCoR: Crosslinked cells were scraped in high SDS lysis buffer (1% SDS, 20mM EDTA, 50mM Tris, pH = 8) and rotated 2h at 4°C to release nuclei. A buffer change was done on pelleted nuclei to the ChIP lysis buffer described above before sonication for 7 cycles (nuclei from approximately 10-12 million crosslinked cells in 0.3 mL lysis buffer was sonicated in 1.5 mL tubes, 30 s on, 30 s off, maximum intensity) in a Bioruptor (Diagenode). Immunoprecipitation was performed overnight using specific antibodies as described below. After washing, IP'ed chromatin was decrosslinked overnight at 65°C, and DNA was purified by phenol-chloroform extraction. Libraries were prepared from the purified DNA using the NEB ChIPseq prep kit, and samples were sequenced according to the manufacturer's instructions (HiSeq v4 Illumina SR sequencing kit).

Antibodies

The following antibodies were used: MED1/TRAP220 M-255 (Santa Cruz, sc-8998), SMC1 (Bethyl Laboratories, Inc; A300-055A), CTCF (Millipore, 07-729), P300 (Santa Cruz, sc-584), HDAC2 (Bethyl Laboratories, Inc; A300-705A), HDAC3 (Santa Cruz, sc-11417), NCoR (Bethyl Laboratories, Inc; A301-145A), H3K27ac (Abcam, ab4729), H3K4me1 (Abcam, ab8895), H3K4me2 (Cell Signaling, 9726). The 4h samples for H3K4me1, H3K4me2, and H3K27ac have been published previously (Siersbæk et al., 2014). The IP and sequencing of the corresponding day 0 samples published here were performed in parallel with the 4h samples. See Table S1 for an overview of ChIP-seq sequencing depth.

mRNA-seq

RNA was harvested at different time points of differentiation in Isol-RNA lysis reagent (5 PRIME). Libraries were prepared from purified RNA (TruSeq Illumina mRNA prep kit) and sequenced according to the manufacturer's instructions (HiSeq v4 Illumina SR sequencing kit). Two different biological replicates were done (i.e., different differentiations). See Table S1 for an overview of mRNA-seq sequencing depth.

QUANTIFICATION AND STATISTICAL ANALYSIS

Topological associating domains (TADs)

Directionality index was calculated using HOMER scoring interactions within 1Mb at a resolution of 50kb using a 5kb moving window (analyzeHiC –boundary 1000000 –superRes 50000 –res 5000). Biased regions were defined as stretches of at least 10 bins with either up- or downstream bias in the entire region and higher absolute bias than 0.5 in at least one bin. Type 1 (T1) boundaries were defined as the start of the bin that transitions between an up- and a downstream biased region, and type 2 (T2) as the start of the bin that transitions between a down- and an upstream biased region. Topological association domains (TADs) were defined as regions that start at a T1 boundary (T1A), crosses a T2 boundary and end at a T1 boundary (T1B). Any TAD with upstream bias between T1A and T2, or downstream bias between T2 and T1B were discarded. The start and end of TADs were defined as the bin with the maximal downstream bias in the region between T1A and T2 and the bin with the maximal upstream bias in the region between T2 and T1B, respectively.

HSV transformation of PCHi-C data

All significant interactions identified by CHiCAGO (Score $\geq$ 5 in at least one condition) were filtered in multiple steps. First, all trans interactions were discarded. Second, interactions spanning more than 1 Mb were discarded. Third, baited ultra-conserved elements were discarded. Fourth, all promoter-promoter interactions were discarded. Fifth, all interactions from non-protein-coding promoters were discarded. Finally, interactions with one of the interacting regions located in regions on chromosome 10 that are amplified in 3T3-L1 cells (chr10:106613366-107858706 and chr10:116174799-118176364) were removed. The tag counts of the remaining 181,093 interactions were TMM normalized using edgeR (Robinson et al., 2010). This procedure yields the normalized tag count for each time point (X_τ). The value (V) was defined as the maximal X_τ across all time points.

$$V = \max_\tau (X_\tau)$$

The saturation (S) is indicative of the maximal fold change between any time points, and was defined such that S · V = max – min:

$$S = 1 - \frac{\min_\tau (X_\tau)}{V}$$

Finally, the hue (H) is indicative of the temporal shape, and was calculated by:

$$H = \left(2 + \frac{X_0 + X_4 - X_{48} - V}{V \cdot S}\right) \cdot 60 \cdot \frac{X_4 - X_0}{|X_4 - X_0|}$$

For illustration purposes, the values of V and S were scaled between 0 and 1 in steps of 0.01 based on rank.

mRNA-seq analyses

mRNA-seq reads were mapped to the genome using STAR (Dobin et al., 2013) and significantly changing genes (Padj $\leq$ 0.01; P value adjusted by FDR) were identified by DESeq2 (Love et al., 2014) after normalizing each library to number of reads in all protein-encoding genes. Fuzzy c-means clustering was performed in R (R Core Team, 2013) to identify robust temporal patterns of gene expression. A gene was accepted into the cluster that provided the strongest membership score, given that each replicate also had the strongest membership score to the same cluster and that the membership score was above 0.3 for the averaged replicates, and above 0.2 for each replicate.

ChIP-seq analyses

50 bp reads were mapped to the genome using STAR (Dobin et al., 2013), and subsequent analyses were performed using a combination of HOMER (Heinz et al., 2010), bedtools (Quinlan and Hall, 2010) and R (R Core Team, 2013). Peak calling was done by HOMER, and significantly changing binding sites (Padj $\leq$ 0.05) were identified by DEseq2 (Love et al., 2014) after normalizing each library to 10M tags. Transcription factor ChIP-seq and input data were obtained from (Siersbæk et al., 2011, GEO: GSE27826; Siersbæk et al., 2014, GEO: GSE56872; Step et al., 2014, GEO: GSE56745).

Calling super-enhancers based on MED1 ChIP-seq data

To only focus on robust MED1 binding sites, we filtered the MED1 binding sites that were identified by HOMER (Heinz et al., 2010) (parameters: -center –size 200 –F 4 –L 4 –fdr 0.0001 –localSize 20000) using a tag count cutoff as previously described (Siersbæk et al., 2014), i.e., peaks of 400 bp should have a tag count of at least 24 tags after normalization of library size to 10M tags. Furthermore, only those binding sites identified in both biological replicates were used in subsequent analyses. Filtered MED1 binding regions within 12.5 kb were merged using bedtools (Quinlan and Hall, 2010), and super-enhancers were called on each time point of differentiation (i.e., day 0, 4h, day 2, day 4, and day 7) using the ROSE package (Lovén et al., 2013; Whyte et al., 2013). Only those regions that were called as super-enhancers in both biological replicates were kept as true super-enhancers. Overlapping super-enhancers from different time points were merged by bedtools (Quinlan and Hall, 2010), tag counts in these merged super-enhancers were determined by HOMER (Heinz et al., 2010), and significantly changing enhancers (Padj $\leq$ 0.05) were identified by DEseq2 (Love et al., 2014). Read counts for these enhancers were subjected to fuzzy c-means clustering in R (R Core Team, 2013). An enhancer was accepted into the cluster that gave the strongest membership score, given that each replicate also had the strongest membership score to the same cluster and that the membership score was above 0.3 for the averaged replicates and above 0.2 for each replicate. For clustering of super-enhancers across only D0, 4h and D2, the enhancers were further trimmed out of clusters if the hue of the enhancer varied more than 20° from the hue of the cluster center.

Calculating enrichment/depletion of interactions at enhancers and gene promoters

Enrichment/depletion of interactions with different temporal profiles at gene promoters in the seven mRNA-seq clusters was calculated as follows. For a defined hue window, the number of interactions connected to genes in a specific cluster as well as interactions connected to the promoters of constitutively expressed genes was determined, and the fraction of those interactions connected to genes in the specific cluster was calculated. The same fraction was calculated for interactions outside the defined hue window. Enrichment/depletion in the defined hue window was then calculated as the ratio of these fractions. This produces enrichment/depletion values that indicate whether interactions for a given cluster more often have a specific temporal profile compared to other profiles and constitutive genes. Hue windows of 40° were used, and they were moved 1° around the hue circle for each enrichment/depletion calculation. Only interactions spanning $\leq$ 100 kb were included in the analyses. The enrichment/depletion of interactions at (super-)enhancers was calculated in a similar manner. For super-enhancers, these calculations were performed at the levels of enhancer constituents, i.e., individual enhancers within larger super-enhancer regions. For a defined hue window, the number of interactions connected to any of the clustered enhancers was determined and the fraction connected to a specific cluster was calculated. The same fraction was calculated for interactions outside the defined hue window and the enrichment/depletion in the defined hue window was calculated as the ratio of these fractions. The rolling hue window was the same as described above for the gene clusters and only interactions spanning $\leq$ 100 kb were included in the analyses. Binomial tests and subsequent FDR correction (using fdrtool in R) was used to identify significantly enriched/depleted hue windows, i.e., interaction profiles (FDR-adjusted P $\leq$ 0.1).

Prediction of dynamic chromatin loops

Corepressor or coactivator peaks were identified over input using HOMER (findPeaks: –size 200 –F 4 –L 4 –fdr 0.0001 –localSize 20000). Broad regions enriched for histone mark occupancy were identified and centered on the most likely nucleosome-free region using HOMER (findPeaks: –region –size 500 –minDist 1000 –nfr –F 4 –fdr 0.0001). The centered broad regions were resized to 500 bp,

and all histone mark and cofactor peaks were merged into a master peak list. Tags were counted and normalized to a total of 10 million tags using HOMER for all cofactors (annotatePeaks: –size 500) and all histone marks (annotatePeaks: –size 5000). The mean of replicates was calculated and $\log_2$ fold changes (LFC) (using 0.25 as a pseudo-count) were calculated for each cofactor or histone mark. The master peak list was overlapped with all PIRs for interactions spanning 250kb or less. The interactions from each PIR fragment were classified as either induced (LFC $\geq$ $\log_2$ (1.5)), repressed (LFC $\leq$ -$\log_2$ (1.5)) or constitutive (|LFC| < $\log_2$ (1.5)). All PIR fragments with constitutive or both induced and repressed interactions were discarded. For each cofactor or histone mark, the dynamics of the chromatin loops were predicted based on the LFC of the cofactor or mark using the pROC package in R (Robin et al., 2011).

Composite corepressor and coactivator scores

Corepressor or coactivator peaks were identified over input using HOMER (findPeaks: –size 200 –F 4 –L 4 –fdr 0.0001 –localSize 20000) and subsequently merged into a master peak list. Tags were counted and normalized to a total of 10 million tags for all corepressors and coactivators in these regions using HOMER (annotatePeaks: –size 500). The mean of replicates was calculated. Weak ($\leq$20 tags / 10 million in the sample with highest occupancy) and clonal ($\geq$100 tags / 10 million in the sample with lowest occupancy) peaks were discarded. Subsequently, $\log_2$ fold changes (using 0.25 as a pseudo-count) were calculated for each cofactor. The $\log_2$ fold changes (LFC) for each cofactor (f) were transformed by standard methods to obtain a factor-specific score (S_F):

$$S_F = \frac{LFC_F - \overline{LFC_F}}{\widehat{\sigma}_{LFC_F}}$$

A composite score was calculated by summation of scores from cofactors belonging to each class (C) of cofactors (i.e., coactivators or corepressors):

$$S_C = \sum_{F \ni C} S_F$$

Allele-specificity of interactions

Promoter-capture reads from the day 0 samples were aligned and quality-filtered using the standard HiCUP pipeline (Wingett et al., 2015), but not deduplicated. mRNA-seq reads and input reads (own data (GSE27826) combined with many other sources: ArrayExpress: E-MTAB-2537 and E-MTAB-1031; GEO: GSE73432, GSE41455, GSE21365, GSE17067, GSE21898, GSE56745, GSE73434, GSE50934, GSE33821, GSE49423, GSE48345) were mapped using the STAR aligner (Dobin et al., 2013). All reads were deduplicated using random selection without considering the mapping score. This is to circumvent the inherent bias from most standard deduplication programs, which keep random reads among the ones with the highest mapping score. The highest mapping score will be found among reads mapped to the reference genome without SNVs, thus biasing the dataset toward the reference genome. From the collapsed PCHi-C and RNA-seq reads, we identified SNVs using Platypus (Rimmer et al., 2014). The SNVs were filtered for sufficient coverage in input data (more than 5 reads covering the SNV). Furthermore, for PCHi-C, we only included SNVs found in either end of significant interactions at day 0, and for RNA-seq, we only included SNVs found in exons. We used the re-mapping approach from WASP (van de Geijn et al., 2015) to control the mapping bias. Using WASP, we tested for allele-selective interactions by testing the allele-balance of reads spanning each interaction and overlapping a specific SNV against the input reads overlapping the same SNV. We tested for allele-selective gene expression by testing the allele-balance of reads spanning SNVs in exons against the input reads overlapping the same SNV. We performed filtering based on blinded variance across both input and either mRNA-seq or PCHi-C data, and FDR-adjusted the P values (using fdrtool in R). To test the enrichment of imbalanced interactions (FDR-adjusted P $\leq$ 0.05) connected to imbalanced genes (FDR-adjusted P $\leq$ 0.05), we performed 100 permutations of selecting distance-matched (+/− 1%) random interactions for each allele-imbalanced interaction and calculated the enrichment of these to the same set of imbalanced genes.

eQTL analysis

We extracted cis-eQTL data from the hypothalamus of mice (Hasin-Brumshtein et al., 2016) and lifted the positions from mm10 to mm9. We filtered the eQTLs to a maximal range of 1Mb (same as the interactions included in the analysis) and kept only the most significant eQTL for each gene. To test the enrichment of eQTLs within interactions connected to the affected gene, we performed 1000 permutations of re-assigning each interaction to a random gene and calculated the enrichment of eQTLs targeting these randomly selected genes.

DATA AND SOFTWARE AVAILABILITY

Data availability

The accession number for the sequence data reported in this paper is GEO: GSE95533.

Code availability

Stand-alone R scripts for full reproduction of main and supplemental figures are publicly available at https://github.com/JesperGrud/PCHiC_3T3L1/.